Nanoscale

Dynamic Article Links

Cite this: *Nanoscale*, 2012, **4**, 2549

www.rsc.org/nanoscale

FEATURE ARTICLE

Critical aspects in the production of periodically ordered mesoporous titania thin films†‡

Galo J. A. A. Soler-Illia,*[a] Paula C. Angelomé,[a] M. Cecilia Fuertes,[a] David Grosso[b] and Cedric Boissiere[b]

Received 21st November 2011, Accepted 7th February 2012
DOI: 10.1039/c2nr11817c

Periodically ordered mesoporous titania thin films (MTTF) present a high surface area, controlled porosity in the 2–20 nm pore diameter range and an amorphous or crystalline inorganic framework. These materials are nowadays routinely prepared by combining soft chemistry and supramolecular templating. Photocatalytic transparent coatings and titania-based solar cells are the immediate promising applications. However, a wealth of new prospective uses have emerged on the horizon, such as advanced catalysts, perm-selective membranes, optical materials based on plasmonics and photonics, metamaterials, biomaterials or new magnetic nanocomposites. Current and novel applications rely on the ultimate control of the materials features such as pore size and geometry, surface functionality and wall structure. Even if a certain control of these characteristics has been provided by the methods reported so far, the needs for the next generation of MTTF require a deeper insight in the physical and chemical processes taking place in their preparation and processing. This article presents a critical discussion of these aspects. This discussion is essential to evolve from know-how to sound knowledge, aiming at a rational materials design of these fascinating systems.

[a]*Gerencia Química, Centro Atómico Constituyentes, Comisión Nacional de Energía Atómica, Av. Gral Paz 1499, B1650KNA San Martín, Buenos Aires, Argentina*
[b]*UPMC Univ. Paris 06, CNRS, UMR 7574, Laboratoire Chimie de la Matière Condensée de Paris, Collège de France, 11 place Marcelin Berthelot, 75005 Paris, France*

† Electronic supplementary information (ESI) available. See DOI: 10.1039/c2nr11817c

‡ Dedicated to Clément Sanchez, on the first anniversary of his appointment to the Hybrid Materials Chair of the Collège de France.

Galo J. A. A. Soler-Illia

Galo Juan de Avila Arturo Soler-Illia was born in Buenos Aires in 1970. He studied chemistry at the University of Buenos Aires (UBA), and worked as a postdoctoral fellow at the University of Paris VI. Since 2003, he has been a CONICET staff scientist at CNEA, Buenos Aires, Argentina, and Professor at the Department of Inorganic Chemistry, UBA. He was awarded several prizes, among them two Houssay Awards in Chemistry (Ministry of Sciences, Argentina), and the Academia Nacional de Ciencias Prize (Argentina). His main current interest is the rational development of novel multifunctional materials with applications in environment, health and energy. More information can be found at http://www.qi.fcen.uba.ar/personales/soler-illia.htm.

Paula C. Angelomé

Paula C. Angelomé was born in Buenos Aires, Argentina in 1979. She obtained a Chemistry degree in 2003 and a PhD in 2008, both from the University of Buenos Aires. Her thesis, under the direction of Prof. Soler-Illia, was focused on the synthesis and characterization of mesoporous thin films, including transition metal oxides and hybrid materials. She was awarded the Leloir Prize for the best chemistry thesis 2006–2008 in Argentina. In 2008, she joined Prof. Liz-Marzán's group at Vigo University, Spain, where she is currently a Postdoctoral Fellow. Her current main interests include synthesis of metallic nanoparticles and their integration in composite materials containing mesoporous oxides.

1.0 Introduction

Nanostructured titanium dioxide is one of the most promising materials for its widespread industrial use in paint, optics, cosmetics, and food science, as well as its prospective applications in advanced technologies such as photocatalysis, photovoltaics, sensing, and electrochromics, which are at the very heart of the environmental and energy challenges of the XXIst century. Nanostructured titania is indeed the most studied photocatalyst, and holds promise for alternative, inexpensive solar cells.[1–3] New promising fields for nanostructured titania that include catalysis, information technology, non-linear optics and implant technology, require its processing as thin films.[4] These applications require stable materials with a well defined crystalline structure, highly controlled crystallite size and shape as well as a high, available surface area and accessible pore networks to ensure contact with catalytic substrates, polymers or nanospecies. In addition, titania thin films are transparent in the visible region, non-toxic and can be fabricated by relatively cheap wet processing methods.

A variety of strategies have been reported that lead to TiO_2 nanostructured films from soft chemistry methods. However, for advanced thin film applications, highly controlled mechanical, optical and structural–textural properties are needed. Production of thin films from nanoparticulate sol processing presents limitations regarding control of film homogeneity and batch-to-batch reproducibility. In addition, the textural porosity resulting from sol–gel processing or nanoparticle aggregation is difficult to control, leading to large pore size distributions in the 2–20 nm range, with irregular interconnections that hinder accessibility to the whole material surface. It is thus important to develop sound methods for the reproducible production of high surface area titania with highly controlled pore size and accessibility.

In this context, ordered mesoporous materials obtained from templating strategies represent an important advance, for all the issues regarding pore control and sample homogeneity can in principle be solved.[5] While a variety of reproducible methods for ordered mesoporous silica production were readily developed,[6–10] much less work was devoted to mesoporous transition metal oxides, and the advance was slower.[11,12] This was mainly due to a lack of extended knowledge about control of the hydrolysis and condensation chemistry of Ti(IV) in the mesoporous materials community. The first reports of mesoporous titania introduced the ligand-assisted templating route,[13] which led to powders with channel-like or lamellar pore structure.[14] Complexing agents such as peroxide,[15] atranes[16] or alkylamines[17,18] were subsequently used as condensation control agents. However, these methods did not permit full control of pore shape, size or organization, nor the production of thin films. Stucky's group introduced an elegant process that used $TiCl_4$ as inorganic precursor, *i.e.*, highly acidic conditions in which the Ti(IV) condensation is hindered.[19,20] This breakthrough permitted highly ordered large-mesopore titania xerogels to be obtained upon evaporation of a volatile solvent by the versatile Evaporation-Induced Self-Assembly (EISA) process.[21] More importantly, this very flexible route opened the

M. Cecilia Fuertes

María Cecilia Fuertes was born in Buenos Aires, Argentina, in 1978. She has a degree in Materials Engineering (1997–2003), from the University of Mar del Plata, and a PhD in Materials Science and Technology (2005–2009) from the Sabato Institute-CNEA and the University of San Martín. Her PhD thesis on the synthesis and characterization of multiscale materials based on mesoporous oxide thin films was advised by G. Soler-Illia. She is a CONICET staff scientist at CNEA, Buenos Aires, Argentina. Her current main interests include the design and production of functional nanomaterials, with applications in (photo)catalysis and optical devices and sensors.

David Grosso

Prof. D. Grosso was appointed as Associate Professor in 2002, and as Professor in 2007, at the University of Paris. He works in the Laboratory Chimie de la Matière Condensée de Paris (LCMCP) on processing nanostructured materials through bottom-up approaches. He is the co-author of more than 100 articles and 10 patents. His work was awarded by the International Sol–gel Society (ISGS) in 2005 and by the French Society of Chemistry (SFC) in 2009. He has been a junior member of the French Institute of Universities since 2009, and he is a co-founder of a start-up "COLIGRO" proposing solutions for chemical surface treatment of stones.

Cedric Boissiere

Cedric Boissiere was born in France, in 1974. He performed his PhD in the European Institute of Membranes, University of Montpellier, in inorganic membranes, for which he was awarded the 2005 prize of the European Membrane Society. After a short postdoctoral position with S. Mann, he became CNRS researcher in 2002, at LCMC, Paris. Since then, his research activities are dedicated to the elaboration of hierarchical, hybrid and inorganic nanomaterials by coupling sol–gel chemistry and smart processes. He is the co-author of more than 80 papers and 15 patents. He was recently honored with the 2007 Jean Rist Medal of the French Society of Materials and Metallurgy.

path to process a variety of silica and non-silica oxides as powders, monoliths or thin films.[22]

The first reports of mesoporous titania thin films (MTTF) either adapted the chloride route,[23] used chelating agents,[24] or utilized pre-formed nanosized titania particle precursors.[25] This first wave of papers presented the structural features, and demonstrated that two main routes were possible, either from molecular or nanoparticulate precursors and non-ionic templates.

After more than a decade, a wealth of work about the production of mesoporous titania has emerged. The prospective applications[26] are the main driving force for the advance in this burgeoning field. A survey of recent literature shows that the focus is at present on the production of MTTF by a variety of means, and in reporting a given property, with no further analysis or thorough comparison with previous work. A lack of discussion on the ultimate mesostructure control is the general rule. It is important to stress that features such as pore size and shape, pore system geometry, surface or the wall crystalline structure are at the origin of the photocatalytic, electron transfer and optical properties or biocompatibility of the final material. At the present state of the art, it would be desirable to concentrate on the actual relationship between synthesis procedures, their role in the final materials structure and the desired properties. This is a general limitation of ongoing work in nanochemistry, as has been signalled by Ozin and Cademartiri:[27] "…attention has been too focused on demonstrating devices and functions, with so called proof-of-concept examples that in many cases end up proving very little in terms of technological potential. […] What is more often needed is a consistent and systematic approach to the understanding of the issues behind the current problems of reproducibility and reliability in nanoscale devices and materials." Consistent with the cited approach, we felt that there is also a lack of consensus on the use and interpretation of characterization techniques. This often leads to confusion in the structure determination, impeding the development of a common ground for the comprehension of the mesopore array and framework features, which is essential to understand the actual properties.

The aim of this paper is not to present an exhaustive discussion of all the work in this exciting and thriving field, as several excellent reviews on the subject are available.[4,26,28] Here, we present the concepts behind MTTF production, and discuss the critical synthesis aspects that influence their structure and properties, supported by an analysis of crossed characterization techniques. We believe that only a deep understanding of these aspects will open the path to rationally designed and tailored MTTFs for advanced applications, and will eventually lead to their massive production at low cost. In addition, we present several cases in which MTTFs act as building blocks of more complex film structures (patterned nanocomposites, multilayers, biohybrids). MTTFs are an example of nanomaterials with tailorable scale-dependent properties that can be rationally designed and eventually integrated in more complex multiscale devices.

2.0 General structural and synthetic aspects

The EISA method involves a cooperative assembly process between sol–gel species and supramolecular templates.[21,29,30] The delicate tuning of the inorganic and organic species that will co-assemble during the coating process is complex, and several forces at different length scales are implicated. Relevant advances took place in the last years through the comprehension of the pore structure, as well as formation paths; yet, systematic research is needed to achieve a complete fine tuning of the mesostructure ordering and orientation, as well as the full pore architecture.[31]

2.1 Overview of an MTTF production process

Mesoporous film production generally implies a sequence of five steps: 1) precursor choice and preparation of the initial solutions, 2) deposition from chemical solutions, 3) controlled post-synthesis aging, 4) template removal, 5) wall crystallization. This sequence is schematised in Fig. 1. It is important to remark here that the processing sequence of MTTF (steps 2–5) is as important towards the final film properties as step 1.

A typical synthesis implies the use of the following components in the precursor solutions: a) a volatile solvent with low surface tension, in order to improve wettability and decrease the reactivity of the inorganic species through dilution, b) an inorganic species, whether molecular, cluster-like or nanosized, c) a supramolecular template (porogen), generally a surfactant, d) an inorganic hydrolysis/condensation agent, such as water, e) a condensation controlling agent. The chemical conditions must be adequately fixed in order to keep the titanium entities as hydrophilic and as small as possible to facilitate the interaction with the hydrophilic part of the surfactant, and to accommodate the high curvature of the micelles during self-assembly.[22,32,33] A central aspect is thus to accurately control the Ti–O–Ti bond formation through polycondensation. When using molecular precursors, this is achieved by using acidic conditions, or by the addition of chelating agents. Synthesis methods have also been developed that use pre-formed building blocks (nanoparticles) as the inorganic precursor; in this case, it is necessary to thoroughly control the nanoparticle size, keeping it much below the gyration radius of the template, with a narrow size distribution. The most usual synthesis routes are presented in Table 1.

2.2 Chemistry of the precursor solutions

The most used molecular precursors towards MTTFs are alkoxides ($Ti(OR)_4$, with RO: ethoxide, i-propoxide, n-butoxide…) or titanium chloride, $TiCl_4$. The first step involves dissolving such precursors in the solvent (alcohols, or a moderately polar solvent such as THF). Titanium alkoxides are extremely hygroscopic and reactive precursors, and a moisture-free environment is usually needed for their handling. On the other hand, titanium chloride is difficult to handle due to its fast and very exothermic hydrolysis reaction with water and damp air. When alkoxides are used, the addition of acid or a chelating agent is necessary. HCl is preferred due to its volatility, which is required during evaporation-assisted deposition. In the case of chloride precursors, alcoholysis or hydrolysis processes release protons that acidify the solution. In both cases, the intermediate precursor has a composition that is governed by the chemical equilibrium existing between the free and the coordinated nucleophilic species (z, u, v, see Fig. 2), while the degree of

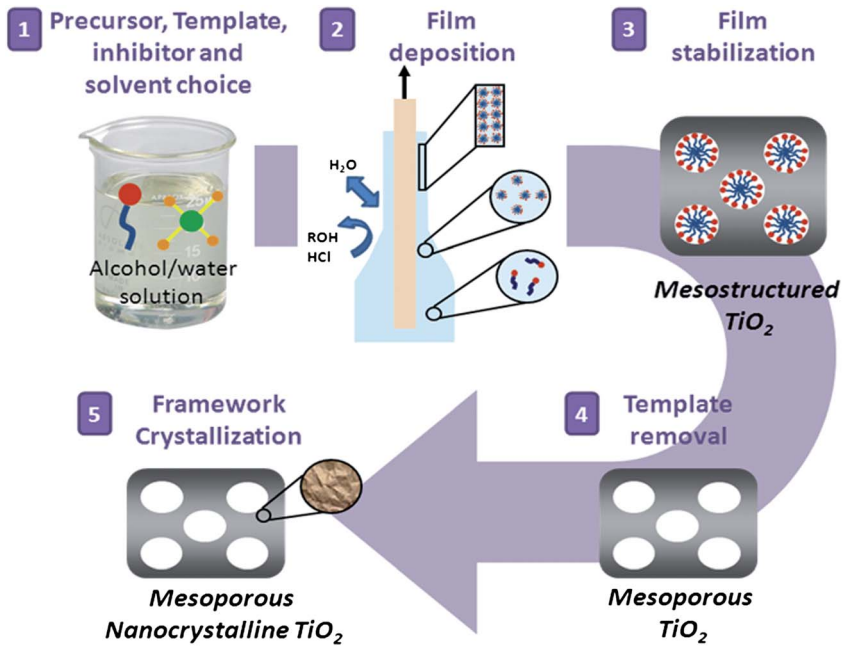

Fig. 1 Scheme of the sequence of steps involved in the production of mesoporous titania thin films (MTTF).

Table 1 Summary of the most usual synthesis routes for MTTF

Year	Precursor	Template	Solvent	T_{max}	Meso/Crystalline	Ref.
2001	$TiCl_4$	Pluronic F127	EtOH	350 °C	*p6m*, amorphous or anatase	34
2001	Titanium isopropoxide	Pluronic P123	2-Propanol	300 °C for 4 h	Thermally induced phase transition from *Pm3n* to a hexagonal structure; anatase	24
2001	Ti NP, $TiCl_4$	Brij	EtOH	450 °C for 5 h	Ordered mesostructure (cubic or 2D hexagonal) determined using XRD and TEM	25
2002	Titanium tetraethoxide + HCl	Pluronic P123	EtOH	400 °C for 4 h; Hex. mesotructure: 250 °C for 4 h	*Im3m*, 2D hexagonal, and lamellar mesostructures. Cubic films with anatase nanocrystalline walls	35
2003	$TiCl_4$	Pluronic F127, Brij 56 or Brij 58	EtOH	350°–400 °C	*Im3m* or *p6m*, amorphous or anatase	36
2003	Ti NP from titanium isopropoxide	Pluronic P123	H_2O	350 °C	Ordered mesostructure but the type of structure is not determined, anatase	37
2004	$TiCl_4$	KLE—PB-PEO	EtOH	700 °C	*Im3m*, anatase	38
2010	$TiCl_4$	Pluronic F127	H_2O	5 min at 500 °C	Gridlike structure formed through the thermally induced transformation of *Im3m*, anatase	39

condensation (x, y) depends mainly on the well known sol–gel ratios $h = [H_2O] : [Ti]$ and $p = [H^+] : [Ti]$.

Tian *et al.* introduced the use of a mixture of alkoxides and chlorides in order to tune the acidity and thus the reactivity of the Ti–oxo species;[40,41] in any case, the use of alkoxides or chlorides yield similar intermediates, since the evolution of Ti^{IV} species is governed by the same chemical exchanges in the same environment. However, the use of different hydrolysis–condensation and aging conditions leads to porous systems with a variety of ordering. Fig. 3a shows solution ^{17}O NMR spectra of acidic solutions of titanium ethoxide with a different $p = [H^+] : [Ti(IV)]$ ratio; this is a useful technique to follow Ti(IV) condensation.[42,43] Solutions with $p = 4$ contain small amounts of Ti–oxo species presenting sharp NMR signals with prevailing μ_2-oxo bridges; in less acidic solutions ($p = 1$), large signals belonging to μ_2-, μ_3- and μ_4-oxo bridges appear, which are typical of more condensed and polydisperse Ti–oxo polymers. Similar results were obtained by analyzing the Ti XANES-EXAFS spectra of the precursor solutions.[36] SAXS patterns of F127-templated films obtained from solutions with $p = 1$ and $p = 4$ and submitted to identical processing conditions are shown in Fig. 3b and 3c, respectively. This demonstrates that the films obtained from smaller, less condensed building blocks present a higher mesostructure ordering. This effect is linked to the higher flexibility of smaller blocks to accompany the template curvature, and to organize more rapidly around the nascent mesostructure upon solvent evaporation. Ageing time is also a relevant factor that influences the Ti–O–Ti condensation process, and care has to be taken of this evolution especially in solutions containing a low quantity of

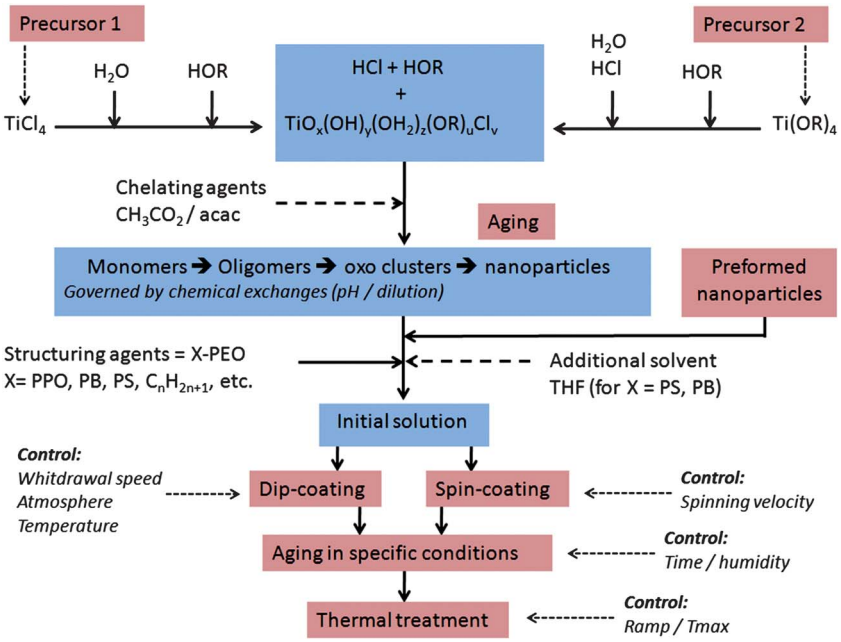

Fig. 2 General paths leading to a MTTF. Ti-intermediate species are composed of partially condensed entities, whose composition (x, y, z, u, v and coordinated chelating agents) is governed by time and the chemical exchange equilibrium between the reactive species in solution. As long as the entities remain hydrophilic and small to adapt to the micelle curvature, a hybrid mesostructure will be formed upon EISA. Upon deposition, the system is still "alive", and ordering can be improved upon ageing under a controlled atmosphere. Thermal treatment will freeze the latter structure into the final mesoporous film.

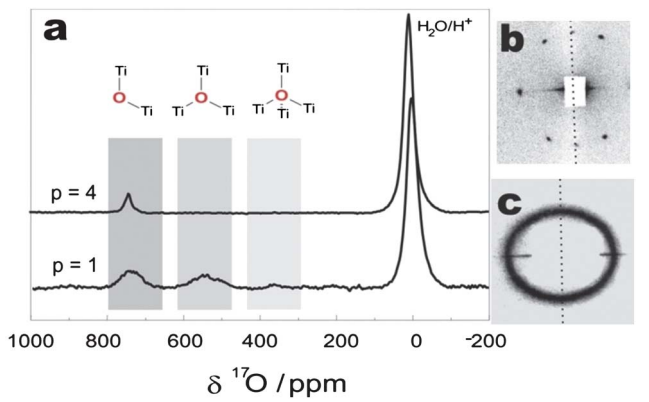

Fig. 3 (a) ^{17}O NMR spectrum of $Ti(OEt)_4$ precursor solutions with $p = [H^+] : [Ti] = 1$ or 4; the resonances corresponding to the Ti–oxo bridges are indicated in the graph; adapted from ref. 36. The SAXS patterns of an MTTF prepared from the different precursor solutions are shown in (b) ($p = 4$) and (c) ($p = 1$).

inhibitor. As a general rule for titania, the higher the condensation extent, the more difficult it is to obtain well-ordered mesostructures in a reproducible way.

Chelating agents such as acetate or β-diketonate have also been be used to control condensation.[24] These are efficient growth inhibitors, leading to organized mesopore arrays, alone or assisted by minor quantities of acid. However, they lead to higher contraction during thermal treatment due to the higher content of organic agents. In summary, disregarding safety, environment and cost issues, alkoxides or chlorides lead to the same intermediates, whose composition is mostly governed by chemical exchanges in solution.

The use of molecular precursors leads in most cases to an MTTF with an amorphous or semicrystalline wall structure when thermally treated at low temperatures. Thus, pre-formed nanocrystalline titania has also been used as an inorganic precursor, in order to attain an MTTF with some crystalline character at relatively low temperatures.[25,37] A pre-synthesis step leads to the production of titania nanoparticles after controlled hydrolysis and condensation. When using this approach, care must be taken in controlling the size and the hydrophilicity of the building blocks. The use of hydrophobic clusters or nanoparticles leads to mesoporous materials with ill-defined, small mesopores; in this case, the added surfactant acts only as a spacer, but not as a pore template.[33] In addition, larger nanoparticles experience higher attractive forces of colloidal origin, and tend to aggregate before film formation. This aspect conspires against attaining a transparent film with regular thickness and high pore ordering.

2.3 The templating agent

The choice of the templating agent is central towards the symmetry of the porous network and the pore size tuning. Fig. 4 shows three examples of the variety of available MTTF porosity architectures. Although mesoporous titania xerogels have been produced using ionic templates such as CTAB,[44] the common characteristic of all successful MTTF syntheses is the use of structure directing agents with non-ionic hydrophilic blocks, in particular the well-known amphiphilic block copolymers (ABC),

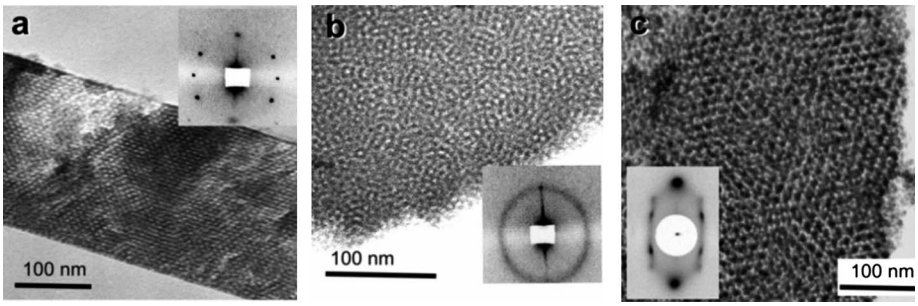

Fig. 4 Transmission electron microscopy (TEM) micrographs of F127-templated titania using (a) $p = 4$, *Im3m* cubic phase (b) $p = 1$ after 48 h solution ageing, local order phase; (c) P123-templated titania using titanium ethoxide in butanol and $p = 1$, *Fm3m* cubic phase. Insets show 2D-SAXS patterns.

which are excellent templates for ordered mesoporous materials.[45,46]

The most common polar head is composed of poly(ethylene oxide) chains (PEO). The hydrophobic region can contain any species that is more hydrophobic than PEO, ranging from alkyl groups (Brij series), poly(propylene oxide) (PPO, Pluronics or Synperonics series), to polystyrene (PS, KLE series),[47] or polyisoprene (PI).[48] PEO is an ideal hydrophilic block, as it can favourably interact with Ti-oxo hydrophilic species in solution and upon drying, stabilising the inorganic–organic interface at the shell of the existing micelles.[32] In addition, PEO blocks can be produced in variable lengths, permitting variation of the template shape. The symmetry of the pore array is mostly determined by the relative size of the hydrophilic and hydrophobic domains of the template. Larger hydrophilic heads lead to higher curvature phases, in agreement to what is proposed for "hard" micelle packing.[49] This can be illustrated by the case of alkyl-PEO surfactants: it was reported that while Brij 58 –$(EO)_{20}$–$C_{16}H_{33}$– leads to an *Im3m* mesopore structure, Brij 56, with a smaller hydrophilic domain, leads to hexagonally packed cylindrical micelles with *p6m* symmetry.[36] In addition, the template : Ti ratio is also a fundamental synthesis variable. It has been demonstrated that increasing s = [P123] : [Ti] ratios gives rise to different pore structures, through a sequence of cubic, 2D-hexagonal and lamellar mesostructures.[35] Experimental evidence collected so far suggests that the final mesostructure is mostly controlled by the relative volume fractions of the hydrophilic and hydrophobic species in the deposited film. These correspond respectively to the inorganic building blocks, water and the hydrophilic domain of the template, and to the hydrophobic region of the template and hydrophobic swelling agents (molecules or polymers). The pore symmetry is mostly insensitive to the nature of the hydrophilic building block that swells the hydrophilic regions of the template, whether this be water or hydrophilic Ti–oxo–hydroxo clusters or nanospecies.[35,36] Regarding pore size control, it is important to note that, although the definition of mesoporous materials include pores in the 2–50 nm range, the most commonly used templating agents give rise to MTTFs with pore diameters below 20 nm. Some strategies to overcome this limit include the use of designed templates or resorting to phase separation methods.[50]

Within this framework, the adequate choice of the precursor and the template : Ti(IV) ratio permits in principle a sort of "thermodynamic design" of the desired mesophase. However, kinetics plays an important role, and the pore topology can also be controlled by the conditions during the deposition and post-treatment steps.

2.4 Chemical solution deposition

Highly ordered MTTFs are mainly obtained by spin- or dip-coating on glass, silicon or conductive substrates such as ITO or FTO. The substrate nature, while being a very important issue in the thermal treatment step (see below), has little influence in the deposition step, although a substrate surface with appropriate wetting is desired. Most of the precursor solutions contain an alcohol as the main solvent due to their low surface tension and high volatility required in any liquid deposition process to avoid dewetting. Film thickness can be adjusted typically in the 50–500 nm range by modifying conditions such as precursor concentration, solution density or viscosity, or by varying processing parameters such as the deposition temperature, the withdrawal speed (dip-coating) or the spinning rate (spin-coating).[51] Films thicker than 500–600 nm are less mechanically stable, and deposition of multilayers is required in order to obtain a crack-free MTTF with thicknesses in the order of microns.

According to interferometry measurements, a micrometre-thick layer of the freshly deposited solution undergoes evaporation, leaving non-volatile inorganic species and the template on the substrate.[52] At this stage, the deposited film is in a relatively viscous liquid-crystal-like phase, the Ti–oxo building blocks remain uncondensed, and the template self-assembly induced by evaporation is triggered. The latter mechanism is thermodynamically and kinetically governed by slight variations of the film composition. This is why efforts have been dedicated to understand and master the role of evaporation rate and composition of the atmosphere in equilibrium with the film composition. Two extreme cases can be distinguished, as sketched in Fig. 5. The first one concerns systems templated by micelles that are already formed in solution (large block copolymers with high hydrophilic contrast, such as poly(ethylene-*co*-butylene)-*b*-poly(ethylene oxide)—the KLE series,[53] or PS-*b*-PEO.[54] Here, the evaporation induces the packing of these into a bcc (*Im3m*) structure with (110) direction perpendicular to the surface. No extra care is required to improve the final order.

The second one concerns most of the cases, when micelles are formed upon, or after, evaporation. In the case of the highly available Pluronics or Brij templates, *in situ* SAXS and interferometry experiments have demonstrated that a local-order

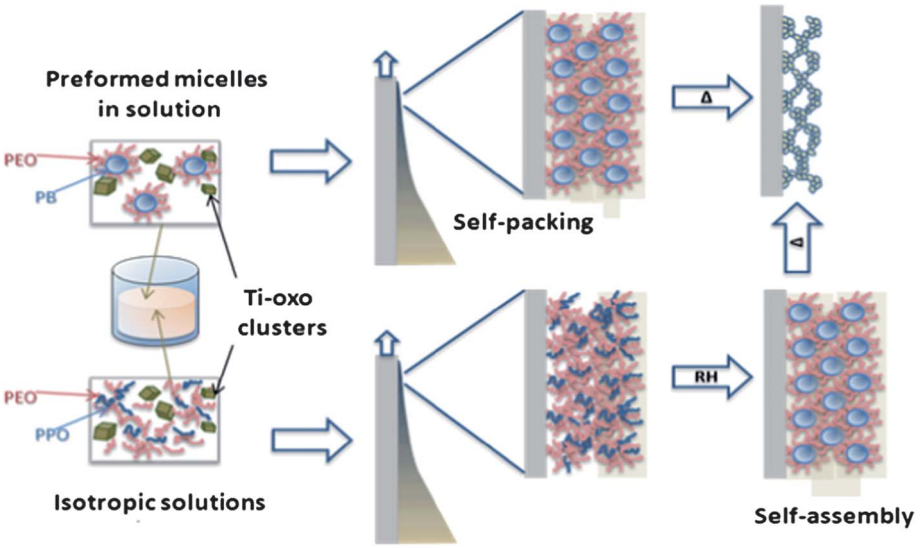

Fig. 5 Scheme of the steps involved in deposition of MTTF from solution in the case of (top) pre-formation of hybrid micelles followed by micelle packing (KLE surfactants) (bottom) evaporation-induced self-assembly. The drawing is not to scale.

mesophase containing template, Ti–oxo nanospecies and acidic water is formed first. This "titanotropic" mesophase[44] remains flexible due to the solvent contents, and the low inorganic condensation.[21] Evolution to a highly ordered hybrid mesophase requires high humidity conditions; under low humidity, the system dries and remains "frozen" into the firstly produced low-order mesophase.[36] The rearrangement kinetics of the block copolymer templates is sluggish, due to their molecular complexity.[46,55] High humidity conditions increase the water content in the firstly formed film, helping to rearrange the template chains, leading to a faster ordering. In order to optimize mesostructure ordering, it has also been proposed to use templates with high hydrophilic–hydrophobic contrast.[30,36] In addition, post-synthetic treatment can also lead to meso-order improvement, as will be discussed in the following section.

Dip-coating is with no doubt the more suitable method to produce these kinds of films because the atmosphere and temperature (key factors in the final structure obtained, see below) can be accurately controlled during the deposition. Simple relationships have been found between the withdrawing speed or solution parameters and the film thickness, no matter the complexity of the system.[56] Moreover, when performed at ultra-low speeds in the capillarity regime, dip-coating is the only method that allows the reproducible deposition of a crack-free, micrometre-thick MTTF from purely aqueous solutions.[39,57]

2.5 Post-deposition processing towards high ordering

Post-treatment of freshly formed films by ageing under controlled external humidity or temperature becomes a crucial step to control the mesostructure order, through a "modulable steady state".[58] Based on the *in situ* measurements, typical post-treatment of titania films consists of a first ageing step at 50% relative humidity atmosphere to optimize the mesophase.[59] While high humidity ageing conditions are in general beneficial as they promote template rearrangement, *in situ* XRR studies showed that prolonged treatments at humidities higher than 70% can be detrimental to the meso-ordering due to excessive water swelling.[60] Instead, prolonged treatments at a RH between 20 and 50% lead to highly ordered MTTFs (see ESI†).[61] These findings support the idea of working under intermediate RH conditions that optimize the trade-off between fast rearrangement kinetics with low mesostructure swelling.

Ageing is followed by a consolidation step: a slow and progressive thermal treatment until 200 °C that locks the desired structure, eliminates microporosity by enhancing the microphase separation of the template, and completes inorganic condensation, ending up with a robust hybrid mesostructured material.[30] Films not submitted to this consolidation step are fragile, and their mesostructure is prone to collapse upon thermal treatment. Nanoparticle-based films need to be kept at low temperatures for longer intervals. This process, while leading to superb order and reproducibility, is time consuming for the construction of devices implying several mesoporous layers (photovoltaic cells, photocatalysis, interferential systems…).

Recently, it was reported that a flash treatment at 500 °C with no previous ageing in high humidity gives similar results to the stabilization sequence if one starts from a purely aqueous solution containing only $TiCl_4$ and F127.[62] The differences and advantages of this approach lie in several points. First, the dip-coating performed with pure aqueous solution requires the deposition to be performed at low speed (usually less than 0.5 mm s^{-1}) in the so-called capillary regime, with the advantage of no substrate dewetting. The evaporation of water is spurred by a moderate heating of the dip-coater chamber (40 to 80 °C). Second, the use of a highly acidic water medium stabilizes hydrophilic titania–oxo clusters, and leads to a faster titania condensation after deposition. Films produced under these specific conditions are already well ordered after coating, thus do not require any humidity stabilisation before the thermal treatment. Hence, this process is adapted to the fast processing of MTTFs.

2.6 Understanding post-deposition processing

Understanding the factors behind post-treatment is essential to design and optimize the processing for obtaining highly organized MTTFs. *In situ* experiments made clear that the freshly produced hybrid mesophase swells under high humidity conditions; this swelling is partially reversible when the RH is lowered. Under controlled humidity ageing, acidity progressively decreases in the film (acid species are washed out), promoting slow condensation and stiffening of the network.[36] An optimized humidity range/temperature/ageing time is needed, to reach order before extended condensation takes place.

New ellipsometry-based experiments can shed light on the influence of water humidity on the ageing of the freshly deposited, uncondensed MTTF. We present here an investigation of the influence of temperature and relative humidity on the kinetics of stabilisation of F127-templated MTTFs. This study permits detection of the sol–gel transition, defined here as the point after which the film can be safely removed from humid air while conserving its mesoscale ordering (in other words, the locking point). The experience consisted on following the evolution of refractive index at 633 nm (n_{633}) and the thickness of an as-made film maintained at a fixed temperature, while the relative humidity (RH) was set at 65%. Every 3 min, the RH was decreased to 25% to monitor its drying–swelling behaviour (see ESI† for experimental details). While this experiment does not reflect the actual film processing sequence, it provides a unique picture of the condensation of the mesostructured phase.

The results obtained for ageing at 30 °C are shown in Fig. 6. At short times, the as-made film behaves like a flexible layer. When the RH is increased from 25 to 65%, a thickness increase of 16% is observed, while n_{633} decreases massively. This indicates that liquid water domains (with a lower refractive index of 1.33) are formed in the deposited layer. This behaviour is typical of a non-cohesive structure, just as the one observed when a low glass transition polymer layer swells in the presence of solvent vapours. Upon one 65%–25%–65% RH cycle, the initial thickness is almost retrieved, and the refractive index slightly increases. Along the first stage of *ca.* 2 h, n increases continuously, and the drying–swelling amplitude decreases. This indicates that the initial mesophase slowly condenses during ageing.

The evolution of n_{633} and thickness along this modulated treatment permits to estimate the sol–gel transition. After 2.35 h at 30 °C, the film presents the same n_{633} at 25% and 65% RH. This critical point, indicated by the first arrow (t_{gel}), is the sign that water does not nucleate anymore within the film, hence a proof that the system is more cohesive due to condensation. After this point, the refractive index decreases every time the RH is decreased to 25%. This is only possible if a significant fraction of the water evaporated from the film is replaced by air, and thus the film structure is rigid enough to resist contraction. Accordingly, the film swelling is much smaller. A second critical point can be defined as the densification time (t_{dens}, second arrow), which is related to the TiO_2 condensation degree. After t_{dens}, a smooth increase in n_{633} is observed, and both curves at 65 and 25% run parallel; the swelling is practically negligible. This indicates the final locking of the titania structure.

A systematic investigation of t_{gel} and t_{dens} values for different ageing temperatures (Fig. 7) shows that both critical values approach each other at higher temperatures. Therefore, the condensation time of the titania framework can be significantly

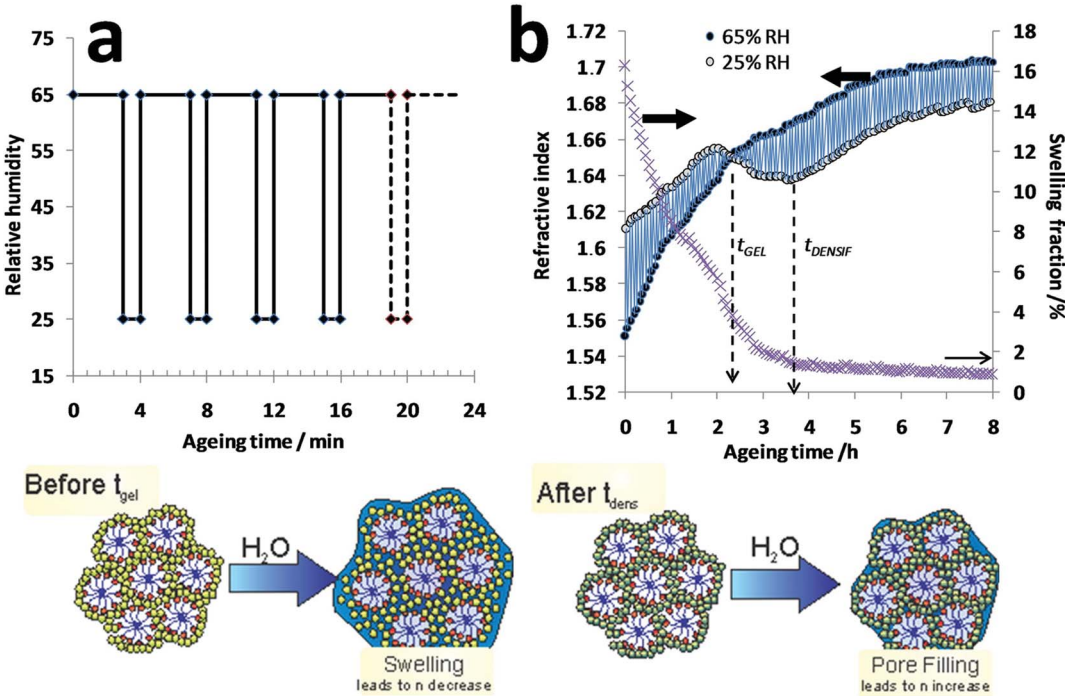

Fig. 6 (a) Relative humidity variation program used in the *in situ* ellipsometry ageing of a freshly deposited titania–template film; $TiCl_4$ was used as precursor, and F127 as the template; (b) refractive index at 633 nm (left axis) and film swelling fraction upon RH change from 25% to 65% (right axis) plotted *versus* ageing time at 30 °C. Closed symbols: n_{633} at 65% RH; open symbols: n_{633} at 25% RH. Arrows mark the t_{gel} and t_{dens}, see discussion in the text. Upon water uptake, mesostructure swelling or pore filling processes take place depending on the framework condensation, as sketched in the lower part.

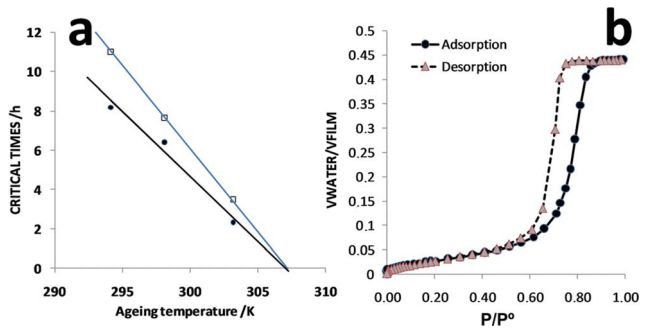

Fig. 7 (a) Plot of t_{gel} (full circle) and t_{dens} (open squares) at different ageing temperatures; (b) water adsorption–desorption isotherm of an F127-templated TiO_2 film aged at 34 °C for 10 min and calcined at 500 °C for 10 min.

decreased from several hours to a very short period, just by ageing the films at slightly higher temperatures. A simple linear fit describes the evolution of both critical times in this temperature range. Fig. 7a clarifies the role of the ambient temperature as a critical parameter for film deposition and ageing. Stabilisation protocols described in the literature do not pay special attention to the ageing temperature, which can vary significantly and lead to the report of different optimal conditions according to the laboratory location. The major conclusion of this experiment is that in principle a well structured and robust film can be produced after a very short stabilisation time if the following rules are obeyed: (i) the RH leading to the structuring of the ordered phase must be maintained for a delay at least equal to t_{dens}; (ii) for very short stabilisation times, the ageing temperature must be equal or higher than a certain temperature. This prediction was proven right by successfully stabilizing an as-made film at RH = 70% and 34 °C in only 10 min. After thermal treatment, the obtained layer presented a good mesostructure quality with a narrow pore size distribution (Fig. 7b).

By extension, this model permits understanding of the highly organised MTTF obtained from water-based dip-coating solutions with no need for thorough ageing under controlled RH%.[61] As this specific process implies slow water evaporation at temperatures higher than 34 °C, the temperature criterion is fulfilled. At the same time, a high relative humidity is present at the drying line, also fulfilling the high relative humidity criterion.

2.7 Thermal treatment

The main properties of MTTFs are directly related to its accessible porosity and the crystalline structure of the walls. Thus, the thermal program applied is of major importance, for it is at the very origin of both aspects. The thermal treatment of F127-templated MTTFs has been thoroughly studied by *in situ* measurements. A sequence of transformation steps has been identified:

a) Framework consolidation by condensation and water release (T < 200 °C). Evaporation of remaining solvent and acid activates framework condensation. This step is accompanied by a *ca.* 25–35% uniaxial shrinkage of the mesostructure along the *z* axis, according to SAXS information.[63]

b) Template removal (250–350 °C). Template pyrolysis generates the porosity, and is accompanied by a further uniaxial shrinkage of *ca.* 20–30%, along with the densification of the inorganic network. Pyrolysis activation energies in the range of 120–130 kcal mol^{-1} were reported.[64]

c) Crystallite nucleation and growth on walls (T > 300 °C). In this temperature range, partially superimposed with the previous one, densification of the titania framework leads to changes in the pore structure. The thermal evolution can be roughly divided into two sub-steps, corresponding to nucleation (300–350 °C) and extensive crystallite growth followed by diffusive sintering (T > 350 °C).[63–65]

Control of this last step is crucial for obtaining the desired final material with nanocrystalline walls and a controlled structure at different length scales. Activation energies of the crystallization process obtained in templated systems using *in situ* XRD or thermal ellipsometry analysis (TEA) are shown in Table 2.

While there is a clear consensus in the evolution to larger pores and interpore necks upon heating, and the important role of confinement in crystallite growth, reports differ in the actual mechanism of nucleation and growth. Kirsch *et al.* propose that anatase crystallization proceeds by a slower nucleation step, occurring preferentially at the interfaces, followed by rapid growth, due to the high surface : volume ratio.[66] If crystallization is controlled by this slower nucleation step, the optimum treatment would imply short time treatments at high temperatures, such as suggested by Grosso *et al.*[63] Instead, Ozin and coworkers propose that a fast nucleation followed by a one-dimensional diffusion controlled crystallite growth takes place. In this case, the pore topology is essential for controlling diffusion.[67] Bass *et al.* subscribe to a low-dimensional diffusion-controlled model, remarking that nucleation might not be a rate determining step;[64] indeed, small anatase-like domains detected by XANES at low temperatures can be considered nucleation centers.[68] It is however clear that extended growth of an anatase nanocrystal network after the nucleation step must be avoided to maintain the ordered porosity.

In all reported successful routes, these aspects have been taken into account. For example, a (110) oriented cubic *Im3m* structure experiences successively unidirectional shrinkage, nucleation-growth and diffusive sintering. This leads to pore merging in the direction of the C_6 axis of the structure, where the interpore walls are thinner.[63] The resulting structure can be defined as a "grid-like" structure with symmetries corresponding to a tetragonal structure. This structure is recognised by the GISAXS diffraction signals corresponding to the lateral periodicity derived from the (1–10) cubic peaks at $q_z = 0$ (Fig. 8). As a result of the sintering process, a high transversal interpore connectivity develops along the film, as proven by the observed evolution of the Type IV adsorption isotherms. The distorted *Im3m* structure obtained at 350 °C presents an H2-type hysteresis loop, typical of mesopores with restrictions. The adsorption–desorption curve of a grid-like mesostructure obtained after a short thermal treatment to 600 °C presents a narrow H1-type loop with parallel branches, closer to the one obtained for open-ended cylindrical pores,[69,70] allowing an optimal molecular transport through the pore system. Due to the importance of crystallinity, the ordering of pre-formed well crystallized anatase nanoparticles using block copolymers was also tested. Nevertheless, recent results indicate that mesoporous films prepared from molecular precursors are more active as

Table 2 Activation energy of anatase nucleation and growth

Mesophase (template)	T Range (°C)	E_{act} (kJ mol^{-1})	Process	Max crystallite size (nm)	Method	Reference
Im3m (P123)	400–450 °C	210 ± 40	Nucleation	9	XRD	66
Im3m (P123)	400–450 °C	140 ± 30	Restructuring	9	XRD	66
P6mm (P123)	350–600 °C	127	Crystallization	14	XRD	67
Im3m (F127)	300–600 °C	185	Crystallization	Not reported	TEA	64

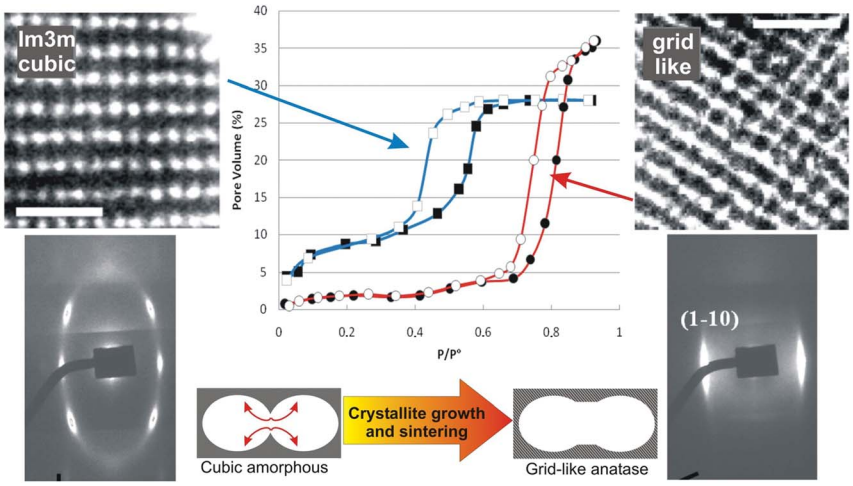

Fig. 8 Evolution from an *Im3m* pore symmetry obtained at 350 °C (left) to grid-like pores obtained at a short treatment at 700 °C (right) mesostructure upon thermal treatment, as witnessed by TEM, SAXS and EP. Data extracted from ref. 65. Scale bars represent 50 nm.

photocatalysts due to a more efficient electronic connectivity between the crystallites.[71]

The substrate also plays a central role in the crystallization step. While anatase crystallization is fast and well defined on silicon for temperatures above 350 °C, it is sluggish on glass or ITO, which delay titania crystallization.[68,72] This is a limitation for applications in solar cells, which require transparent electrodes. To overcome this issue, several strategies have been developed: depositing a dense underlayer,[73] or submitting to high temperatures for short times ("flash treatment")[65] lead to improved crystallinity. The drawback of the second method is its reproducibility, particularly for high temperature treatment.

Mastering the thermal processing of MTTFs is fundamental in order to obtain highly ordered mesoporous materials with nanocrystalline walls. An optimized thermal program should maintain the ordered pore array after template elimination, and limit the crystallite growth in such a way that the order is not disrupted. In addition, if this process can be shortened, the preparation time of multilayer systems including MTTFs would become more attractive for industrial production.

3.0 Characterisation: the need for crossing information

In view of the tailorability required for MTTF applications, it is necessary to deeply characterize their structure at the atomic and mesoscopic level, such as: type of pore array, physical thickness, porosity (pore volume, pore size distribution, interconnectivity, specific surface area), surface topography and philicity, chemical composition, and crystallinity. In addition, it is essential to cross-confirm these characteristics by sophisticated techniques, in order to have a full comprehension of the structure–properties relationships that are crucial for a rational materials design.

The most commonly used characterization techniques for MTTFs are presented in Fig. 9. Several techniques belonging to the scattering, spectroscopy and imaging families are basically employed; most of them have to be sensitive to the very small film mass deposited onto a bulk substrate, which is in the order of 0.1 mg cm^{-2}. Spectroscopic techniques used to assess the main features of MTTFs include UV-visible spectroscopy or ellipsometry (E) (film band gap, Ti(IV) environment), Fourier-transform infrared spectroscopy, FTIR (presence of template, or organic groups), Raman spectroscopy (titania crystalline phase by analyzing the Ti–O–Ti vibrations in the 200–600 cm^{-1} region),[74] X-Ray photoelectron spectroscopy, XPS (surface, presence and speciation of organic groups, see ref. 75). X-Ray absorption techniques like XANES and EXAFS have been used to accurately characterize the Ti(IV) environment in solution and in the final material, although they generally require synchrotron facilities, which is somewhat of a limitation.[36,68]

In addition, *in situ* studies have been introduced to shed light into the processes that take place upon film deposition or thermal treatment, which are central to optimize the production of MTTFs. Synchrotron 2D small angle X-Ray scattering (2D-SAXS), interferometry and ellipsometry are fast enough techniques, and were successfully used to follow the EISA, ageing and thermal treatment steps.[23,76] *In situ* time-resolved 2D-SAXS has been employed to follow the evolution of the titania–template

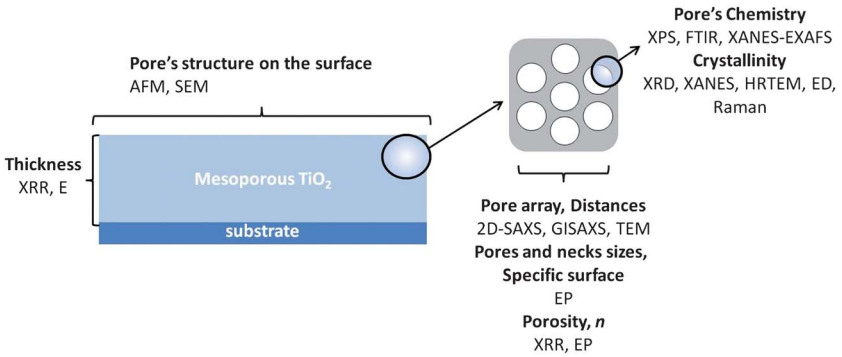

Fig. 9 Characterisation techniques most commonly used and information provided.

mesophase straight after dip-coating, and during thermal treatment, coupled to XRD.[65] TEA was used to follow the refractive index and the thickness of the films during annealing.[64] The resulting deep understanding of the intimate formation and evolution mechanisms permitted the definition of robust and reproducible synthesis procedures.[36,63]

While a thorough overview of characterization techniques for mesoporous thin films has been presented elsewhere,[4] we will focus below on relevant examples that illustrate the importance of crossed characterization in MTTFs.

3.1 The complete structural characterization of an *Im3m* cubic mesostructure

2D-SAXS provides the full diffraction patterns from which the space group, the lattice parameters, the domain orientation and the circular permutation of the corresponding pore array structure can be deduced.[77] The results are representative of the whole sample since the data are collected on a large portion of the film. It is important to note that film analysis by X-Ray diffraction (XRD) in Bragg-Brentano geometry (*i.e.*, 1D low angle XRD) will only provide information about the periodicity in the direction normal to the surface of the substrate. Microscopies such as SEM, TEM or AFM are local techniques, and should be used as a complementary technique to diffraction, but in no case should a structure determination be based only on these results.

Indeed, combined SAXS and electronic microscopy permits unambiguous determination of the spatial pore arrangement. SAXS patterns obtained at 3° incidence of an F127-templated MTTF just after film preparation show a set of diffraction spots that correspond to the plane families {110} and {200} of a body centered cubic structure *Im3m*, oriented with the [110] plane parallel to the films surface and the [1–10] perpendicular to that surface (Fig. 10a). Normal transmission measurements (90° incidence, Fig. 10a) yield diffraction rings at the same {110} distances. Analysis of the whole SAXS information establishes that the pore system presents *Im3m* ordered domains in the z direction and randomly oriented in the xy direction (Fig. 10b).[36,78]

Upon stabilization and thermal treatment of the films, a uniaxial shrinkage along the z is observed, due to the adhesion of the film to the substrate (Fig. 10c). The resulting structure is a triclinic P1 phase.[79] However, it is more convenient to describe it as a contracted *Im3m* structure and continue to use the cubic plane assignment, extracting a cubic structure parameter of $a_{SAXS} = 17.7 \pm 0.6$ nm from the in-plane spots (*i.e.*, $q_z = 0$, see Fig. 10d).

Top-view TEM micrographs of *Im3m*-derived MTTFs usually present a "modulated channel pattern" (Fig. 10e) that often leads to erroneous interpretations. Taking into account the information provided by 2D-SAXS, the "modulated channels" are in fact the projection of superimposed pores of [110] planes perpendicularly oriented to the surface (Fig. 10f). Pores have a low density and are transparent to the electron beam. The walls of the "channels" present the same periodicity of the [110] planes, and the cubic structural parameter obtained from TEM is $a_{TEM} = 18 \pm 1$ nm.

Scanning electron microscopy (SEM) shows the actual surface pore arrangement (Fig. 10g). The Fourier transformed picture (Fig. 10h) of a mono-oriented region shows six spots at two different distances to the FT, with a 0.88 ratio between the short and long distances, close to the expected 0.87 theoretical distance ratio expected for a [110] face (Fig. 10i). The cubic parameter obtained from the SEM image is $a_{SAXS} = 19 \pm 2$ nm, in excellent agreement with TEM and 2D-SAXS data. This "4 + 2" array should not be confused with a hexagonal arrangement (observed in *Fm3m*, for example), where the expected ratio is 1.

3.2 Determination of film porosity: ellipsometric porosimetry (EP) and X-Ray reflectometry (XRR)

MTTF porosity is one of the most important quantities to be determined, yet one of the most elusive, due to the low material amount present in the film. Nitrogen adsorption requires several milligrams of sample for an accurate measurement, which implies scratching a high number of film samples. N_2-BET analysis on powders prepared by drying cast solutions (*i.e.*, xerogels) do not provide accurate pore volume or size values, due to differences in drying and contraction between supported and non-supported mesoporous samples, which present a different evolution of the inorganic condensation upon thermal treatment.[80,81]

Ellipsometry (E) is a reliable optical technique for film characterization that permits determination of film thickness and refractive index, $n(\lambda)$. Ellipsometric porosimetry (EP) has been developed to assess the porosity of mesoporous thin films.

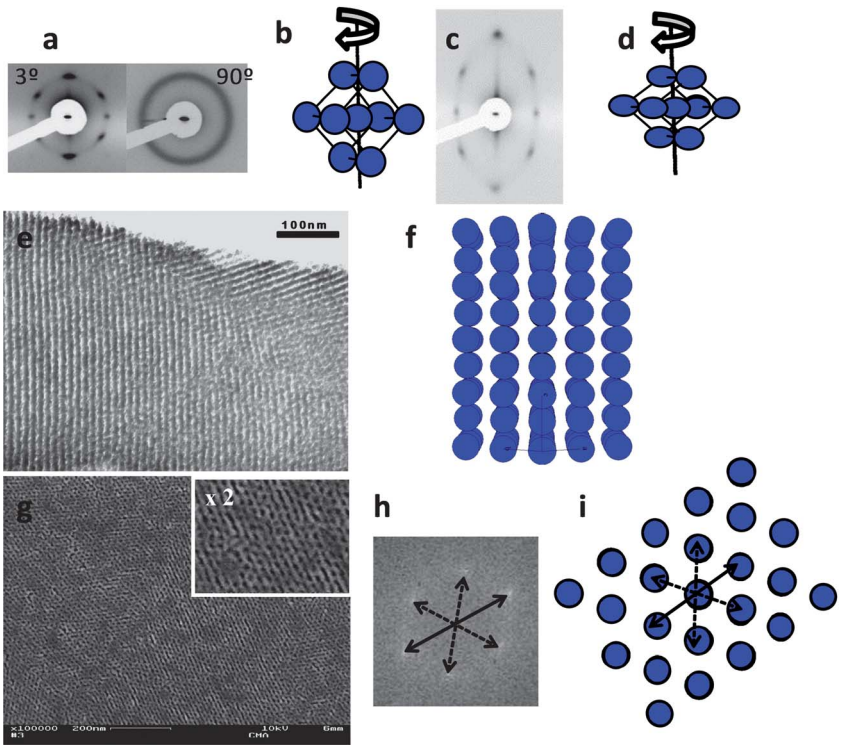

Fig. 10 (a) 2D-SAXS pattern (at 3° and 90°) of an F127-templated MTTF as prepared, (b) representation of *Im3m* cubic structure, (c) 2D-SAXS pattern of the same film after a thermal treatment up to 200 °C, (d) representation of *Im3m* cubic structure uniaxially contracted in the *z* direction, (e) TEM image of the same film, (f) projection of the *Im3m* cubic phase oriented in [110] direction, (g) SEM image of the surface of the same film, (h) Fourier transform of image presented in (g), and (i) [110] plane of *Im3m* cubic structure. In all the schemes the blue spheres represent the pores.

EP consists of measuring the variation of film refractive index exposed to a given vapour, as a function of the partial vapour pressure, P/P^{sat}. Solvent adsorption isotherms can be obtained, and the accessible pore volume, pore size and pore size distribution can be estimated using a simple model that uses Kelvin's law (Fig. 11a).[82] Pore interconnectivity and specific surface area can also be obtained from EP analysis, under gas flux.[83] EP measurements are performed in a swift manner, but results are model-dependent, in particular, pore shape has to be estimated. In addition, the most used solvent is water, which is straightforward from the operational point of view, but a complex adsorbate, particularly on oxides. Accurate surface energies of water and titania are needed to perform a t-plot analysis, to obtain reliable surface areas and pore sizes. This aspect is somehow lacking in the current methods, and is not found in the literature, somehow limiting the application of EP as an absolute method. However, EP is excellent for obtaining a fast comparison between different synthesis conditions.

X-Ray reflectometry (XRR) can be used to independently obtain the parameters obtained by EP.[84–86] The reflectivity critical angle θ_c allows a direct determination of the film electronic density; film thickness is separately obtained from the Kiessig interference fringes. This information, combined with the results for dense films can be used to determine the accessible and the total film porosity (Fig. 11b). Changes in the film electronic density along water adsorption can be directly obtained from the evaluation of θ_c.[85] EP and XRR give coincident results, as shown for Brij58-templated TiO_2 films in Fig. 11 and Table 3.

3.3 The wall nature: XRD *versus* spectroscopy

A wealth of efforts is devoted to characterize the wall crystalline structure of the inorganic framework, which is an essential feature of MTTFs in view of their applications. XRD is the best suited tool for crystallinity evaluation, *i.e.*, phase and crystallite size. Most works present the evolution of XRD peak intensity and width, which give a broad idea of crystalline character and an estimation of crystallite growth, respectively. However, sol–gel derived titania walls are constituted by nanocrystalline and amorphous domains, and it is important to be able to quantify the amount of crystalline character of MTTFs. This can be achieved by a diversity of techniques as spectroscopy (as discussed below) or even electrochemical analysis.[53]

Angelomé *et al.*[68] have proposed the use of XANES spectroscopy to measure the amount of anatase present in MTTFs during thermal treatment. The analysis of the pre-edge zone in the XANES spectra allowed the study of the Ti local symmetry, and accurate quantification of the crystalline fraction of the inorganic walls. This technique demonstrated that a small fraction of anatase-like domains is present from temperatures as low as 200 °C, and that there is a direct relation between the crystalline character and the photodegradation of salicylic acid (Fig. 12). Coincidentally, Vansant and co-workers have determined that a small fraction of anatase is present at low temperature treatments, depending on the experimental conditions, using *in situ* Raman spectroscopy to follow crystallization in mesoporous titania powders;[87,88] this technique is also useful for

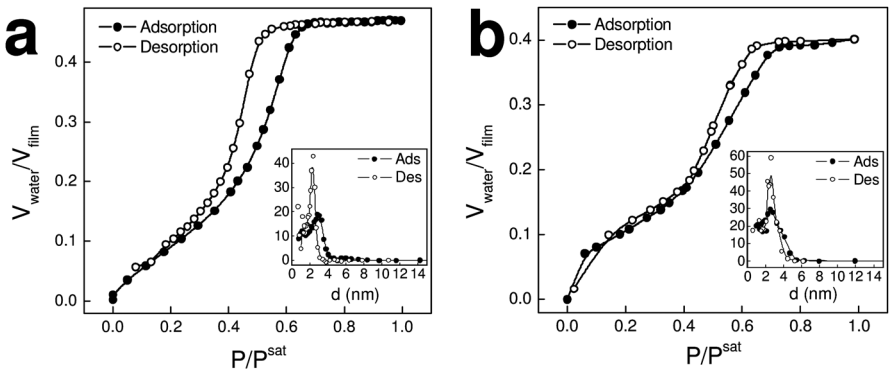

Fig. 11 Water adsorption–desorption isotherms for a Brij58-templated TiO_2 film obtained using (a) EP and (b) XRR. Insets: pore size distributions calculated from the corresponding isotherms.

Table 3 Thicknesses, accessible porosities (P_A), pore's small diameters (d_{pore}) and neck's diameters (d_{neck}) of a Brij58-templated TiO_2 film obtained using XRR and EP. The pore's large diameters values (D_{pore}) are obtained considering the film contraction (~60%), previously determined by 2D-SAXS

Technique	Thickness (nm)	P_A (%)	D_{pore} (nm)	d_{pore} (nm)	d_{neck} (nm)
EP	130	47	4.6	2.8	2.3
XRR	131	40	4.3	2.6	2.5

film characterization,[89] and the analysis of peak shift and breadth has been applied to characterize the appearance, confined growth and defects of crystalline phases.[72]

4.0 Beyond MTTF

In the previous sections, we have shown the chemical and processing strategies to prepare MTTFs by the usual templating routes. If the reader takes into account that only a small number of relatively well-known systems were presented and analyzed, it is clear that the possibilities opened by combining the co-assembly of inorganic and organic building blocks are practically limited by the imagination. Indeed, a wide range of MTTF-based systems with exciting properties is available by modifying the preparation protocols, by incorporating other templating methods, or by combining MTTFs with other suitable nano-building blocks, as schematized in Fig. 13. This section will briefly comment on new developments based on such modified systems.

4.1 Ultrathin mesoporous TiO_2 layers

Adjusting the chemical and processing conditions allowing perfect tuning of the film thickness. A minimal thickness is reached when both viscous drag and capillary regimes are equally overlapping at a critical withdrawal speed that usually stands close to 0.2 mm s^{-1}. Under these conditions, ultrathin TiO_2 layers (4–15 nm thick) bearing ordered nanoperforations (10–80 nm in diameter) through which the surface of the substrate (*e.g.* Si,

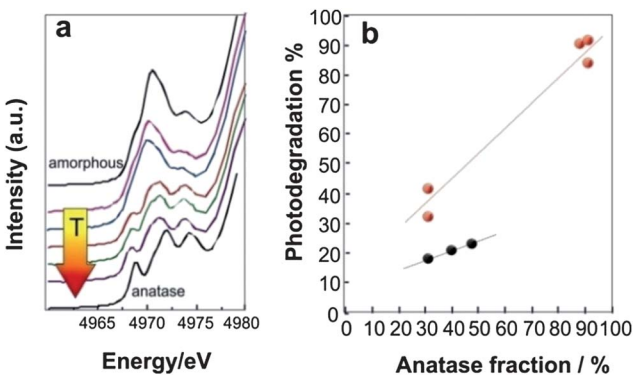

Fig. 12 (a) Ti K XANES spectra of MTTF deposited onto Si substrates, spectra in black correspond to amorphous and crystalline anatase TiO_2; curves depict the evolution from 300 to 450 °C. (b) Correlation between salicylate photodegradation and anatase fraction. Red circles: Si-supported MTTF, black circles: ITO-supported MTTF; dotted lines are a guide for the eye. Adapted from ref. 68.

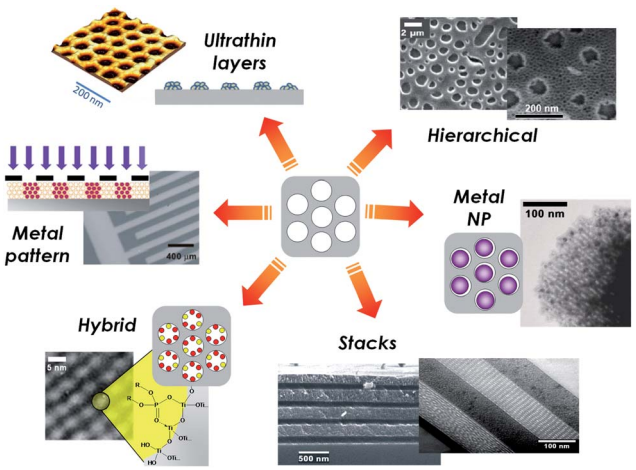

Fig. 13 Scheme of the possibilities beyond MTTF.

glass, FTO, ITO, Au, *etc.*) is accessible can be produced. Upon thermal treatment, crystallisation and diffusive sintering lead to the formation of ordered patterns that have been used as substrates for selective local growth of nano-objects for data storage systems.[90] They have also been used as surfaces with controlled wetting properties, as components for antireflective self-cleaning layers, or to prepared ultra nano-electrode arrays. More recently, deep-X-ray lithography was applied to these systems to perform nano-in-micro patterns.[91]

4.2 Hierarchically porous titania

Expanding the mesopore diameter beyond 10 nm and obtaining hierarchically porous materials is a challenge for applications based on mesoporous thin films, especially in systems that need enhanced transport properties or those dealing with large molecules such as in nanofluidics or biotechnology. In the case of MTTFs, strategies involve incorporating a second templating strategy that should not interfere with supramolecular templating. The methods for producing hierarchical meso–mesoporous or meso–macroporous thin films have been recently reviewed.[50] Controlled phase separation processes imply harnessing a delicate balance between the solubility of a solvent or polymeric phase in the final film upon evaporation. Titania thin films with macropores and nested mesopores can be obtained by using poly(ethylene glycol) as a phase separation agent, leading to MTTFs presenting macropores with controllable diameters between 0.1 and 2 μm and a mesoporous inorganic wall with an interpore separation of 3–4 nm.[92] In the same vein, a simple one-pot synthesis method that combines supramolecular templating and phase separation has been presented, allowing a meso–mesoporous film with tuned bimodal pore populations to be obtained (small pores 13–18 nm diameter, and large pores 20–150 nm diameter) by controlling the solubility of a pore enhancement agent in the presence of a co-solvent.[93] Interestingly, the larger pores of these films can host large enzymes such as DNA polymerase, which can perform DNA amplification when incubated under polymerase-chain-reaction conditions.[94] Replication of a sacrificial underlayer is another suitable strategy towards multiscale patterns.[95] Mesoporous TiO_2 pillared planar nanochannels were obtained by replication of a PS ordered perforated layer template using a typical $TiCl_4$–F127 system. The final material is composed of an ordered array of vertical mesoporous pillars supporting a continuous roof of the same material, and opens the gate for applications in nanofluidics.[96]

4.3 Hybrid mesoporous titania

A wealth of applications in the fields of magnetic, optoelectronic and photovoltaic materials can be envisioned for materials that combine the variety of properties provided by organic molecules and the electronic properties of TiO_2.[4,97] As no Ti equivalent of the stable silanes X_3Si–R is available, the main alternatives to obtain titania based hybrids are: 1) post functionalization by complexation of Ti(IV), 2) adsorption by electrostatics and 3) infiltration. The complexation case is the more interesting, as the strength of the Ti–organic bond can be controlled by changing the grafting group. Phosphates, carboxylates or phenols were used as anchoring agents, and a binding stability trend was determined: $R–O–PO_3^{2-} \approx R–PO_3^{2-}$ > dicarboxylate > carboxylate.[98,99] These results open up the use of organically modified TiO_2 in a wide variety of applications depending on the bond strength, from controlled release devices to perm-selective membranes.[100,101] This complexation approach can also be used to control the pore size and surface charge of the TiO_2. Taffa *et al.*,[102] have demonstrated that the electrochemical behaviour of a modified electrode towards highly charged electroactive probes depends on the charge of the phosphate attached to the oxide.

Adsorption of organic molecules by electrostatic interactions has also been tested, giving rise to electrochromically active materials.[103,104] These experiments, and a related one with the materials obtained by complexation,[100] demonstrate the electrical contact between adsorbed organic molecules, the TiO_2 and the electrode, paving the way for preparation of dye sensitized solar cells (DSSC). The same electrostatic or complexation interactions described above can be exploited in order to attach molecules to nanocrystalline TiO_2 and then degrade them by means of a photocatalytic process. Applications in solar cells have also inspired the development of polymer-containing MTTFs based on either infiltration of poly(3-hexyl tiophene)[105] or polymerization of pyrrole within the pore system.[106]

4.4 Nanoparticles embedded in mesoporous TiO_2

MTTFs are attractive matrices for the inclusion of nanoparticles (NP), permitting the development and full exploitation of optical, electronic or catalytic properties.[107,108] Metallic or semiconductive NP embedded into a matrix can present tailored plasmonic properties, as well as cooperative matrix-NP effects in catalytic or photochromic materials. Ag NPs can be deposited within TiO_2 mesoporous films through electroless deposition, using a strong reducing agent such as borohydride, or a mild one such as formaldehyde.[109,110]

It is especially interesting to note that including Au or Ag NP in the framework or inside the pores of MTTFs has been demonstrated to improve the electron migration from the semiconductor surface to the metal, which suppresses the electron-hole recombination, one of the main causes of the loss of activity of TiO_2 as a photocatalytic material.[111–114]

4.5 Mesoporous film stacks

The integration of MTTFs in mesoporous multilayered stacks with high accessibility has been used to take advantage of TiO_2 properties (*i.e.* high n and selective reactivity). One-dimensional photonic crystals with very high reflectance at a given wavelength can be built from mesoporous multilayers.[115–119] The n of each layer can change with external conditions, for example, in the presence of vapours. In addition, one particular layer of this photonic crystal can be selectively functionalized by post-grafting molecules. In mesoporous multilayers composed of titania and silica, the different reactivity of each oxide permits the location of chemical functions only on one kind of layer, leading to a selective response towards vapours.[95,115] The concept of selective reactivity was also used to create metallic NP–mesoporous oxide nanocomposites. Reduction of silver ions by formaldehyde proceeds readily onto titania surfaces, but is a slow reaction on silica. Therefore, it is possible to locate Ag NPs

within a titania layer, while leaving the silica pores untouched.[109] This enhanced reactivity was exploited by developing a photocatalytic-assisted lithography process (PAMPA) to produce metallic NP arrays positioned into the titania component of mesoporous silica–titania bilayers,[120] which permitted conductive silver patterns to be obtained within MTTFs.[121]

5.0 Conclusions and outlook: critical aspects for nanoscale control of MTTF

In this paper, we have presented and discussed the phenomena involved in the production of MTTFs. The central questions that have to be raised and studied imply the control of pore topology, dimensions and connectivity, wall thickness and crystalline structure, and the possibility of pore modification, as schematized in Fig. 14.

These features are not independent, but they are spatially correlated at different length scales, and define regions in space with different functionalities. These regions permit integration of active species such as molecules, nanoparticles or surface functions; the properties of the ensemble will be relative to the synergy between each component functionality and their relative spatial location.[122] Mesoporous materials are in some way akin to proteins in that they present "functional domains", nanoscale size regions with highly controlled chemistry and well-defined positional relationship and interactions between them.[123] The fine tuning of these functional and positional features is essential for advanced applications. Indeed, the whole MTTF can be considered an "organized functional nanofacility".[30] These complex architectures can be designed and built through the judicious choice of precursors and adequate processing, which in turn implies mastering a delicate balance of interactions in multicomponent reactive systems with a complex evolution.[29,124] It is clear that optimized conditions for the fabrication of MTTFs are needed, and that they depend on the desired application.

The attempt of tailoring one aspect such as wall crystallinity involves modifying the size, connectivity and accessibility of the whole pore system. A clear example is the case of photocatalysis, in which nanoanatase walls are recognized as the most important factor for the final film performance.[28] The thermal treatment must be carefully controlled in order to obtain both high crystallinity and high available surface area.[65,68,125,126] Higher calcination temperatures lead to more extended crystallinity (*i.e.*, higher anatase fraction, larger crystallites) and open porosity, but also to loss of surface area due to confined growth. Efforts are thus devoted to optimize both aspects by separating nucleation and growth of the anatase crystallites. Crystallization leads to a clear wall rearrangement, enlarging the pore and neck size, until a critical temperature, after which surface area is progressively lost.[65] The influence of the substrate in the deposition and thermal evolution must also be taken into account, especially when aiming at transparent, inexpensive electrodes.

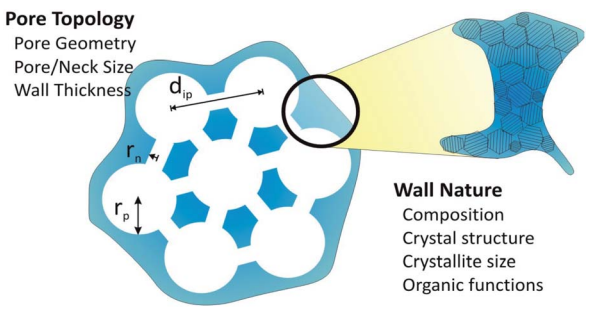

Fig. 14 Relevant functional domains (*i.e.*, regions of space with well-defined features) of MTTFs, and its associated controllable properties.

In the photocatalysis case, however, there are other key factors to control, such as the mesostructure order and pore accessibility. Recent works performed with powder mesoporous titania systems assign an equivalent importance to crystallinity and accessible porosity in the photocatalysis process.[127,128] In the case of films, ordered MTTFs are more active than non-ordered porous ones, and cubic structures are more efficient than hexagonal ones, in both cases due to improved molecule diffusion to the active centres.[65,112,125,126] Again, optimisation of the synthesis design (*i.e.*, choice of the porogen, template : precursor ratio, stabilization process and post-treatment) permits the achievement of highly accessible pore structures with better performance.

Other strategies to obtain higher photocatalytic activities involve surface modification and/or pore filling. Some examples are: pore filling with carbon,[129] doping with nitrogen,[130,131] changing the surface philicity[112,132] and including metal nanoparticles (Au and Ag) in the framework or inside the pores to sensitize the titania.[111–114] These works indicate once again that controlling the reactivity of MTTFs is a key factor in achieving the desired performance.

Another example of the influence of synthesis and processing conditions in the final material properties is the production of MTTF-based solar cells, particularly in DSSCs. The anatase contents and the accessibility of the electrolyte or the electroactive polymer to the mesopore system are the key issues. In addition, the pore surface holds a relevant role, as it determines the organic–inorganic interface in which the electron transfer takes place. Grätzel-type cells with liquid electrolytes using MTTFs reached conversion efficiencies in the order of 4–5%, and improved solar conversion.[133,134] The interconnectivity of the porous system has to be designed to maximize electrolyte–titania contact. Also, one of the most important parameters in this application is the film thickness, which is related to the actual cell power output and conversion efficiency. In this area, there is room for improvement; typical deposition methods, including multilayers, can yield so far micron-thick mesoporous coatings. There is a need for the development of sound methods for the deposition of thicker films, either monolayer or multilayered, in which crystallinity and porosity are regular throughout the film thickness. This can be attained through the understanding and exploitation of the full potential of liquid deposition methods. Indeed, thick and crack-free films can be obtained by dip-coating under appropriately controlled conditions.[135] As the liquid DSSCs are prone to suffer leakage and photocorrosion, the development of all-solid state DSSCs in which the liquid electrolyte is replaced by a polymeric hole carrier is a promising area. These cells are obtained by infiltration of an electroactive polymer and present so far more modest efficiencies in the order of 0.7–3%.[105,136,137] In these systems, the pore size is critical, in order to maximize polymer conjugation, thus enhancing efficiency.[3] A final limitation of ordered MTTFs in solar cell applications is the

deposition of highly crystalline and regular films onto inexpensive transparent and conductive substrates. Deposition on flexible substrates that do not degrade during template removal or thermal treatments is also a desired feature.

However, photocatalytic and solar cell applications are just the tip of the iceberg, in which the ultimate control of pore architecture or even size is not so critical. Advanced prospective applications of MTTFs imply the development of accessible porosity and a very precise tailoring of the high surface area. Simultaneous control of pore accessibility and crystalline wall structure has proven decisive in the Li-insertion properties into MTTFs, aiming at fast charge–discharge electrochromic or energy storage devices.[53,138] In addition, the demonstrated stability of highly porous MTTFs in biological media opens opportunities for applications in the biomaterials field.[139] Metal-deposited MTTFs present quick bone bonding, biological stability and the capability of hosting molecules for drug delivery, which are dependent on pore size and geometry.[140] Perm-selective membranes with complex embedded nanosystems (molecules, polymers, or biomolecules) are also an example in which delicate interactions at the nanoscale have to be managed in order to get a fully functional material.[94,141] Optical MTTF-based materials with new features such as fully aligned channels[142] or tailored plasmons[143] point to the next generation of plasmonic coatings and metamaterials.

The complex interplay of the structural evolution upon film synthesis and processing almost always leads to compromising solutions. The processing aspects (*i.e.*, precursors and templates, number of processing steps, time at each temperature, maximum calcination temperature, *etc.*), have to be optimized for each device in order to lower costs and look forward to industrial production. This permanent necessity for a trade-off raises questions such as: is pore order always necessary, or are high accessibility/porosity and shorter processing times more important? Is it always necessary to have a high anatase fraction, or are lower processing temperatures more convenient? These questions will always be answered by taking into account the final properties needed for a specific application.

The analysis presented here for MTTFs is general, and could be applied to other oxide-based systems by reviewing and analyzing the same factors. The importance of understanding the critical aspects for MTTF synthesis is that it provides rational tools to design these nanomaterials, and to use them in more complex applications. To this end, comprehensive and systematic work is still needed in order to determine basic yet unknown physical–chemical properties of MTTFs. For example, precise assessment of pore size and shape depends on the accurate determination of surface energies and surface group speciation, and on improving the imaging capabilities (*i.e.,* use of micro-tomography). In addition, sound models of molecule behaviour within pores (*i.e.*, molecule condensation, transport, conformations, *etc.*) constitute an important area to be developed. These advances are crucial to develop real sound knowledge about nanoconfinement effects, which constitute the next generation of properties to be pursued. Although nowadays the necessity of developing applications is leading the field, it is crucial to consider the "behind the scenes" of successful nanodevices: the basic research, which ensures the reproducible production of materials with the desired properties.

Acknowledgements

The authors are indebted to ECOS A08E05 and EULASUR projects for travel funding, to ABTLuS for facilitating access to LNLS (SAXS and XRR measurements) and to ANPCyT (PICT 2008-1848 and 2010-0026, FSNANO 2010/007) for general funding. MCF and GJAASI are CONICET researchers. Ianina Violi is gratefully thanked for critically reading this manuscript.

References

1 X. Chen and S. S. Mao, *Chem. Rev.*, 2007, **107**, 2891–2959.
2 M. Grätzel, *Acc. Chem. Res.*, 2009, **42**, 1788–1798.
3 M. D. McGehee, *MRS Bull.*, 2009, **34**, 95–100.
4 C. Sanchez, C. Boissiere, D. Grosso, C. Laberty and L. Nicole, *Chem. Mater.*, 2008, **20**, 682–737.
5 M. Jaroniec and F. Schüth, *Chem. Mater.*, 2008, **20**, 599.
6 C. T. Kresge, M. E. Leonowicz, W. J. Roth, J. C. Vartuli and J. S. Beck, *Nature*, 1992, **359**, 710–712.
7 S. A. Bagshaw, E. Prouzet and T. J. Pinnavaia, *Science*, 1995, **269**, 1242–1244.
8 H. Yang, A. Kuperman, N. Coombs, S. Mamiche Afara and G. A. Ozin, *Nature*, 1996, **379**, 703–705.
9 G. S. Attard, J. C. Glyde and C. G. Goltner, *Nature*, 1995, **378**, 366–368.
10 S. L. Burkett, S. D. Sims and S. Mann, *Chem. Commun.*, 1996, 1367–1368.
11 F. Schüth, *Chem. Mater.*, 2001, **13**, 3184–3195.
12 C. Yu, B. Z. Tian and D. Y. Zhao, *Curr. Opin. Solid State Mater. Sci.*, 2003, **7**, 191–197.
13 D. M. Antonelli and J. Y. Ying, *Angew. Chem. Int. Ed.*, 1995, **34**, 2014–2017.
14 R. L. Putnam, N. Nakagawa, K. M. McGrath, N. Yao, I. A. Aksay, S. M. Gruner and A. Navrotsky, *Chem. Mater.*, 1997, **9**, 2690.
15 D. T. On, *Langmuir*, 1999, **15**, 8561.
16 S. Cabrera, J. El-Haskouri, C. Guillem, J. Latorre, A. Beltrán-Porter, M. D. Marcos and P. Amorós, *Solid State Sci.*, 2000, **2**, 405.
17 N. Ulapaggan and C. N. R. Rao, *Chem. Commun.*, 1996, 1685–1686.
18 D. M. Antonelli, *Microporous Mesoporous Mater.*, 1999, **30**, 315.
19 P. Yang, D. Zhao, D. I. Margolese, B. F. Chmelka and G. D. Stucky, *Nature*, 1998, **396**, 152–155.
20 P. Yang, D. Zhao, D. I. Margolese, B. F. Chmelka and G. D. Stucky, *Chem. Mater.*, 1999, **11**, 2813–2826.
21 C. J. Brinker, Y. Lu, A. Sellinger and H. Fan, *Adv. Mater.*, 1999, **11**, 579–585.
22 D. Grosso, F. Cagnol, G. J. A. A. Soler-Illia, E. L. Crepaldi, H. Amenitsch, A. Brunet-Bruneau, A. Bourgeois and C. Sanchez, *Adv. Funct. Mater.*, 2004, **14**, 309.
23 D. Grosso, A. R. Balkenende, P. A. Albouy, A. Ayral, H. Amenitsch and F. Babonneau, *Chem. Mater.*, 2001, **13**, 1848–1856.
24 H. S. Yun, K. Miyazawa, H. Zhou, I. Honma and M. Kuwabara, *Adv. Mater.*, 2001, **13**, 1377–1380.
25 Y. K. Hwang, K. C. Lee and Y. U. Kwon, *Chem. Commun.*, 2001, 1738–1739.
26 J. H. Pan, X. S. Zhao and W. I. Lee, *Chem. Eng. J.*, 2011, **170**, 363–380.
27 G. A. Ozin and L. Cademartiri, *Small*, 2009, **5**, 1240–1244.
28 M. A. Henderson, *Surf. Sci. Rep.*, 2011, **66**, 185–297.
29 G. J. A. A. Soler-Illia, C. Sanchez, B. Lebeau and J. Patarin, *Chem. Rev.*, 2002, **102**, 4093–4138.
30 G. J. A. A. Soler-Illia and P. Innocenzi, *Chem.–Eur. J.*, 2006, **12**, 4478–4494.
31 P. Innocenzi, L. Malfatti, T. Kidchob and P. Falcaro, *Chem. Mater.*, 2009, **21**, 2555–2564.
32 G. J. A. A. Soler-Illia and C. Sanchez, *New J. Chem.*, 2000, **24**, 493–499.
33 G. J. A. A. Soler-Illia, E. Scolan, A. Louis, P. A. Albouy and C. Sanchez, *New J. Chem.*, 2001, **25**, 156.
34 D. Grosso, G. J. A. A. Soler-Illia, F. Babonneau, C. Sanchez, P. A. Albouy, A. Brunet-Bruneau and A. R. Balkenende, *Adv. Mater.*, 2001, **13**, 1085.
35 P. C. A. Alberius, K. L. Frindell, R. C. Hayward, E. J. Kramer, G. D. Stucky and B. F. Chmelka, *Chem. Mater.*, 2002, **14**, 3284.

36 E. L. Crepaldi, G. J. A. A. Soler-Illia, D. Grosso, F. Cagnol, F. Ribot and C. Sanchez, *J. Am. Chem. Soc.*, 2003, **125**, 9770–9786.
37 F. Bosc, A. Ayral, P. A. Albouy and C. Guizard, *Chem. Mater.*, 2003, **15**, 2463–2468.
38 B. Smarsly, D. Grosso, T. Brezesinski, N. Pinna, C. Boissiere, M. Antonietti and C. Sánchez, *Chem. Mater.*, 2004, **16**, 2948.
39 N. Krins, M. Faustini, B. Louis and D. Grosso, *Chem. Mater.*, 2010, **22**, 6218–6220.
40 B. Z. Tian, H. Yang, X. Liu, S. Xie, C. Yu, J. Fan, B. Tu and D. Y. Zhao, *Chem. Commun.*, 2002, 1824–1825.
41 B. Z. Tian, X. Liu, B. Tu, C. Yu, J. Fan, L. Wang, S. Xie, G. D. Stucky and D. Y. Zhao, *Nat. Mater.*, 2003, **2**, 159–163.
42 V. W. Day, T. A. Eberspacher, Y. Chen, J. Hao and W. G. Klemperer, *Inorg. Chim. Acta*, 1995, **229**, 391–405.
43 J. Blanchard, F. Ribot, C. Sanchez, P.-V. Bellot and A. Trokiner, *J. Non-Cryst. Solids*, 2000, **265**, 83–97.
44 G. J. A. A. Soler-Illia, A. Louis and C. Sanchez, *Chem. Mater.*, 2002, **14**, 750–759.
45 G. J. A. A. Soler-Illia, E. L. Crepaldi, D. Grosso and C. Sanchez, *Curr. Opin. Colloid Interface Sci.*, 2003, **8**, 109–126.
46 F. S. Bates and G. H. Fredrickson, *Phys. Today*, 1999, **52**, 32–38.
47 A. Thomas, H. Schlaad, B. Smarsly and M. Antonietti, *Langmuir*, 2003, **19**, 4455–4459.
48 M. Nedelcu, J. Lee, E. J. W. Crossland, S. C. Warren, M. C. Orilall, S. Guldin, S. Hüttner, C. Ducati, D. Eder, U. Wiesner, U. Steiner and H. J. Snaith, *Soft Matter*, 2009, **5**, 134–139.
49 J. N. Israelachvili, *Intermolecular and surface forces*, Academic Press, Amsterdam, 3rd edn, 2011, pp. 538.
50 P. Innocenzi, L. Malfatti and G. J. A. A. Soler-Illia, *Chem. Mater.*, 2011, **23**, 2501–2509.
51 C. J. Brinker and G. W. Scherer, *Sol–gel science: the physics and chemistry of sol–gel processing*, Academic Press, London, 1990.
52 D. Grosso, F. Babonneau, P.-A. Albouy, H. Amenitsch, A. R. Balkenende, A. Brunet-Bruneau and J. Rivory, *Chem. Mater.*, 2002, **14**, 931–939.
53 D. Fattakhova-Rohlfing, M. Wark, T. Brezesinski, B. M. Smarsly and J. Rathouský, *Adv. Funct. Mater.*, 2007, **17**, 123–132.
54 Y.-J. Cheng and J. S. Gutmann, *J. Am. Chem. Soc.*, 2006, **128**, 4658–4674.
55 G. Karlström, in *Amphiphilic block copolymers self-assembly and applications*, ed. P. Alexandridis and B. Lindmann, Elsevier, Amsterdam, 2000, pp. 41–55.
56 L. C. Huang, E. K. Richman, B. L. Kirsch and S. H. Tolbert, *Microporous Mesoporous Mater.*, 2006, **96**, 341–349.
57 M. Faustini, B. Louis, P.-A. Albouy, M. Kuemmel and D. Grosso, *J. Phys. Chem. C*, 2010, **114**, 7637–7645.
58 F. Cagnol, D. Grosso, G. J. d. A. A. Soler-Illia, E. L. Crepaldi, F. Babonneau, H. Amenitsch and C. Sanchez, *J. Mater. Chem.*, 2003, **13**, 61–66.
59 E. L. Crepaldi, G. J. A. A. Soler-Illia, D. Grosso and C. Sanchez, *New J. Chem.*, 2003, **27**, 9.
60 M. J. Henderson, A. Gibaud, J.-F. Bardeau and J. W. White, *J. Mater. Chem.*, 2006, **16**, 2478–2484.
61 P. C. Angelomé, PhD thesis, *Films delgados mesoporosos de óxidos metálicos, mixtos e híbridos. Hacia un diseño racional de nanomateriales funcionales*, Universidad de Buenos Aires, 2008.
62 M. Faustini, B. Louis, P. A. Albouy, M. Kuemmel and D. Grosso, *J. Phys. Chem. C*, 2010, **114**, 7637–7645.
63 D. Grosso, G. J. A. A. Soler-Illia, E. Crepaldi, F. Cagnol, C. Sinturel, A. Bourgeois, A. Brunet-Bruneau, H. Amenitsch, P. A. Albouy and C. Sanchez, *Chem. Mater.*, 2003, **15**, 4562–4570.
64 J. D. Bass, D. Grosso, C. Boissiere and C. Sanchez, *J. Am. Chem. Soc.*, 2008, **130**, 7882–7897.
65 Y. Sakatani, D. Grosso, L. Nicole, C. Boissiere, G. J. de A. A. Soler-Illia and C. Sanchez, *J. Mater. Chem.*, 2006, **16**, 77–82.
66 B. L. Kirsch, E. K. Richman, A. E. Riley and S. H. Tolbert, *J. Phys. Chem. B*, 2004, **108**, 12698–12706.
67 S. Y. Choi, M. Mamak, S. Speakman, N. Chopra and G. A. Ozin, *Small*, 2005, **1**, 226–232.
68 P. C. Angelomé, L. Andrini, M. E. Calvo, F. G. Requejo, S. A. Bilmes and G. J. A. A. Soler-Illia, *J. Phys. Chem. C*, 2007, **111**, 10886–10893.
69 F. Rouquerol, J. Rouquerol and K. Sing, *Adsorption by powders & porous solids. Principles, methodology and applications*, Academic Press, San Diego, 1999, pp. 204.
70 S. Lowell, J. E. Shields, M. A. Thomas and M. Thommes, *Characterization of porous solids and powders: surface area, porosity and density*, Springer, Dordrecht , 2006.
71 P. Hartmann, D.-K. Lee, B. M. Smarsly and J. Janek, *ACS Nano*, 2010, **4**, 3147–3154.
72 Y. Zhang, J. Li and J. K. Wang, *Chem. Mater.*, 2006, **18**, 2917–2923.
73 U. L. Štangar, U. Černigoj, P. Trebše, K. Maver and S. Gross, *Monatsh. Chem.*, 2006, **137**, 647–655.
74 M. S. Wainwright and N. R. Foster, *Catal. Rev. Sci. Eng.*, 1979, **19**, 211–292.
75 A. Calvo, P. C. Angelomé, V. M. Sánchez, D. A. Scherlis, F. J. Williams and G. J. A. A. Soler-Illia, *Chem. Mater.*, 2008, **20**, 4661–4668.
76 Y. Lu, R. Ganguli, C. A. Drewien, M. T. Anderson, C. J. Brinker, W. Gong, Y. Guo, H. Soyez, B. Dunn, M. H. Huang and J. I. Zink, *Nature*, 1997, **389**.
77 M. Klotz, P.-A. Albouy, A. Ayral, C. Menager, D. Grosso, A. Van der Lee, V. Cabuil, F. Babonneau and C. Guizard, *Chem. Mater.*, 2000, **12**, 1721–1728.
78 G. J. A. A. Soler-Illia, E. L. Crepaldi, D. Grosso, D. Durand and C. Sanchez, *Chem. Commun.*, 2002, 2298–2299.
79 M. P. Tate, V. N. Urade, J. D. Kowalski, T. C. Wei, B. D. Hamilton, B. W. Eggiman and H. W. Hillhouse, *J. Phys. Chem. B*, 2006, **110**, 9882–9892.
80 M. Mazaj, S. Costacurta, N. Zabukovec Logar, G. Mali, N. Novak Tušar, P. Innocenzi, L. Malfatti, F. Thibault-Starzyk, H. Amenitsch, V. Kaučič and G. J. A. A. Soler-Illia, *Langmuir*, 2008, **24**, 6220–6225.
81 G. Mali, M. Mazaj, M. Rangus, G. J. A. A. Soler-Illia and V. Kaučič, *Stud. Surf. Sci. Catal.*, 2008, **174**, 949–952.
82 M. R. Baklanov, K. P. Mogilnikov, V. G. Polovinkin and F. N. Dultsev, *J. Vac. Sci. Technol., B*, 2000, **18**, 1385–1391.
83 C. Boissiere, D. Grosso, S. Lepoutre, L. Nicole, A. B. Bruneau and C. Sanchez, *Langmuir*, 2005, **21**, 12362–12371.
84 A. Gibaud and G. Vignaud, in *X-Ray and neutron reflectivity. Principles and applications*, ed. J. Daillant and A. Gibaud, Springer, Berlin, 2009, pp. 85.
85 A. Gibaud, S. Dourdain and G. Vignaud, *Appl. Surf. Sci.*, 2006, **253**, 3–11.
86 M. Klotz, V. Rouessac, D. Rébiscoul, A. Ayral and A. van der Lee, *Thin Solid Films*, 2006, **495**, 214–218.
87 K. Cassiers, T. Linssen, M. Mathieu, Y. Q. Bai, H. Y. Zhu, P. Cool and E. F. Vansant, *J. Phys. Chem. B*, 2004, **108**, 3713–3721.
88 E. Beyers, P. Cool and E. F. Vansant, *J. Phys. Chem. B*, 2005, **109**, 10081–10086.
89 L. Zhao, Y. Yu, L. Song, X. Hu and A. Larbot, *Appl. Surf. Sci.*, 2005, **239**, 285–291.
90 A. Fisher, M. Kuemmel, M. Järn, M. Lindén, C. Boissiere, L. Nicole, C. Sanchez and D. Grosso, *Small*, 2006, 2.
91 M. Faustini, B. Marmiroli, L. Malfatti, B. Louis, N. Krins, P. Falcaro, G. Grenci, C. Laberty-Robert, H. Amenitsch, P. Innocenzi and D. Grosso, *J. Mater. Chem.*, 2011, **21**, 3597–3603.
92 M. C. Fuertes and G. J. A. A. Soler-Illia, *Chem. Mater.*, 2006, **18**, 2109–2117.
93 L. Malfatti, M. G. Bellino, P. Innocenzi and G. J. A. A. Soler-Illia, *Chem. Mater.*, 2009, **21**, 2763–2769.
94 M. G. Bellino, I. Tropper, H. Duran, A. E. Regazzoni and G. J. A. A. Soler-Illia, *Small*, 2010, **6**, 1221–1225.
95 P. C. Angelomé, M. C. Fuertes and G. J. A. A. Soler-Illia, *Adv. Mater.*, 2006, **18**, 2397–2402.
96 M. Faustini, M. Vayer, B. Marmiroli, M. Hillmyer, H. Amenitsch, C. Sinturel and D. Grosso, *Chem. Mater.*, 2010, **22**, 5687–5694.
97 L. Nicole, C. Boissiere, D. Grosso, A. Quach and C. Sanchez, *J. Mater. Chem.*, 2005, **15**, 3598–3627.
98 P. C. Angelomé, S. Aldabe-Bilmes, M. E. Calvo, E. L. Crepaldi, D. Grosso, C. Sanchez and G. J. A. A. Soler-Illia, *New J. Chem.*, 2005, **29**, 59–63.
99 P. C. Angelomé and G. J. A. A. Soler-Illia, *Chem. Mater.*, 2005, **17**, 322–331.
100 E. Martinez-Ferrero, D. Grosso, C. Boissiere, C. Sanchez, O. Oms, D. Leclercq, A. Vioux, F. Miomandre and P. Audebert, *J. Mater. Chem.*, 2006, **16**, 3762–3767.
101 M. Gaitán, V. R. Gonçales, G. J. A. A. Soler-Illia, L. M. Baraldo and S. I. C. de Torresi, *Biosens. Bioelectron.*, 2010, **26**, 890–893.
102 D. H. Taffa, M. Kathiresan, L. Walder, B. Seelandt and M. Wark, *Phys. Chem. Chem. Phys.*, 2010, **12**, 1473–1482.

103 S. Y. Choi, M. Mamak, N. Coombs, N. Chopra and G. A. Ozin, *Nano Lett.*, 2004, **4**, 1231–1235.
104 H. Jheong, Y. Kim, J. Pan, T.-Y. Won and W. Lee, *J. Electroceram.*, 2006, **17**, 929–932.
105 K. M. Coakley, Y. Liu, M. D. McGehee, K. L. Frindell and G. D. Stucky, *Adv. Funct. Mater.*, 2003, **13**, 301–306.
106 N. C. Strandwitz, Y. Nonoguchi, S. W. Boettcher and G. D. Stucky, *Langmuir*, 2010, **26**, 5319–5322.
107 M. D. Pérez, E. Otal, S. A. Bilmes, G. J. A. A. Soler-Illia, E. L. Crepaldi, D. Grosso and C. Sanchez, *Langmuir*, 2004, **20**, 6879–6886.
108 S. B. Zhang, J. K. Wang, H. T. Liu and X. L. Wang, *Catal. Commun.*, 2008, **9**, 995–1000.
109 M. C. Fuertes, M. Marchena, M. C. Marchi, A. Wolosiuk and G. J. A. A. Soler-Illia, *Small*, 2009, **5**, 272–280.
110 L. Bois, F. Chassagneux, Y. Battie, F. Bessueille, L. Mollet, S. Parola, N. Destouches, N. Toulhoat and N. Moncoffre, *Langmuir*, 2010, **26**, 1199–1206.
111 M. Andersson, H. Birkedal, N. R. Franklin, T. Ostomel, S. Boettcher, A. E. C. Palmqvist and G. D. Stucky, *Chem. Mater.*, 2005, **17**, 1409–1415.
112 I. Bannat, K. Wessels, T. Oekermann, J. Rathousky, D. Bahnemann and M. Wark, *Chem. Mater.*, 2009, **21**, 1645–1653.
113 M.-A. Cha, C. Shin, D. Kannaiyan, Y. H. Jang, S. T. Kochuveedu, D. Y. Ryu and D. H. Kim, *J. Mater. Chem.*, 2009, **19**, 7245–7250.
114 J. Zhao, S. Sallard, B. M. Smarsly, S. Gross, M. Bertino, C. Boissiere, H. Chen and J. Shi, *J. Mater. Chem.*, 2010, **20**, 2831–2839.
115 M. C. Fuertes, F. J. López-Alcaraz, M. C. Marchi, H. E. Troiani, V. Luca, H. Míguez and G. J. D. A. A. Soler-Illia, *Adv. Funct. Mater.*, 2007, **17**, 1247–1254.
116 M. C. Fuertes, S. Colodrero, G. Lozano, A. R. González-Elipe, D. Grosso, C. Boissiere, C. Sanchez, G. J. D. A. A. Soler-Illia and H. Míguez, *J. Phys. Chem. C*, 2008, **112**, 3157–3163.
117 N. Hidalgo, M. E. Calvo and H. Míguez, *Small*, 2009, **5**, 2309–2315.
118 B. V. Lotsch and G. A. Ozin, *Adv. Mater.*, 2008, **20**, 4079.
119 S. Y. Choi, M. Mamak, G. von Freymann, N. Chopra and G. A. Ozin, *Nano Lett.*, 2006, **6**, 2456.
120 E. D. Martínez, M. G. Bellino and G. J. A. A. Soler-Illia, *ACS Appl. Mater. Interfaces*, 2009, **1**, 746.
121 E. D. Martínez, L. Granja, M. G. Bellino and G. J. A. A. Soler-Illia, *Phys. Chem. Chem. Phys.*, 2010, **12**, 14445–14448.
122 M. H. Bartl, S. W. Boettcher, K. L. Frindell and G. D. Stucky, *Acc. Chem. Res.*, 2005, **38**, 263–271.
123 G. J. A. A. Soler-Illia and O. Azzaroni, *Chem. Soc. Rev.*, 2011, **40**, 1107–1150.
124 Y. Wan, H. Yang and D. Y. Zhao, *Acc. Chem. Res.*, 2006, **39**, 423–432.
125 J. C. Yu, X. Wang and X. Fu, *Chem. Mater.*, 2004, **16**, 1523–1530.
126 M. A. Carreon, S. Y. Choi, M. Mamak, N. Chopra and G. A. Ozin, *J. Mater. Chem.*, 2007, **17**, 82–89.
127 A. A. Ismail, D. W. Bahnemann, L. Robben, V. Yarovyi and M. Wark, *Chem. Mater.*, 2010, **22**, 108–116.
128 P. Z. Araujo, V. Luca, P. B. Bozzano, H. L. Bianchi, G. J. A. A. Soler-Illia and M. A. Blesa, *ACS Appl. Mater. Interfaces*, 2010, **2**, 1663–1673.
129 J. Tang, Y. Wu, E. W. McFarland and G. D. Stucky, *Chem. Commun.*, 2004, 1670–1671.
130 S. S. Soni, M. J. Henderson, J.-F. Bardeau and A. Gibaud, *Adv. Mater.*, 2008, **20**, 1493–1498.
131 E. Martinez-Ferrero, Y. Sakatani, C. Boissiere, D. Grosso, A. Fuertes, J. Fraxedas and C. Sanchez, *Adv. Funct. Mater.*, 2007, **17**, 3348–3354.
132 M. Wark, J. Tschirch, O. Bartels, D. Bahnemann and J. Rathouský, *Microporous Mesoporous Mater.*, 2005, **84**, 247–253.
133 M. Zukalová, A. Zukal, L. Kavan, M. K. Nazeeruddin, P. Liska and M. Grätzel, *Nano Lett.*, 2005, **5**, 1789.
134 M. Zukalová, J. Procházka, A. Zukal, J. H. Yum, L. Kavan and M. Grätzel, *J. Electrochem. Soc.*, 2010, **157**, H99–H103.
135 D. Grosso, *J. Mater. Chem.*, 2011, **21**, 17033–17038.
136 K. M. Coakley and M. D. McGehee, *Appl. Phys. Lett.*, 2003, **83**, 3380–3382.
137 K. M. Coakley and M. D. McGehee, *Chem. Mater.*, 2004, **16**, 4533–4542.
138 T. Brezesinski, J. Wang, J. Polleux, B. Dunn and S. H. Tolbert, *J. Am. Chem. Soc.*, 2009, **131**, 1802–1809.
139 J. D. Bass, D. Grosso, C. Boissiere, E. Belamie, T. Coradin and C. Sanchez, *Chem. Mater.*, 2007, **19**, 4349–4356.
140 W. Xia, K. Grandfield, A. Hoess, A. Ballo, Y. Cai and H. Engqvist, *J Biomed Mater Res Part B*, 2011, **100B**, 82–93.
141 G. J. A. A. Soler-Illia, P. C. Angelomé, M. C. Fuertes, A. Calvo, A. Wolosiuk, A. Zelcer, M. G. Bellino and E. D. Martínez, *J. Sol-Gel Sci. Technol.*, 2011, **57**, 299–312.
142 H. Miyata, Y. Fukushima, K. Okamoto, M. Takahashi, M. Watanabe, W. Kubo, A. Komoto, S. Kitamura, Y. Kanno and K. Kuroda, *J. Am. Chem. Soc.*, 2011, **133**, 13539–13544.
143 M. S. Son, J. E. Im, K. K. Wang, S. L. Oh, Y. R. Kim and K. H. Yoo, *Appl. Phys. Lett.*, 2010, **96**, 023115–023117.

